

STEP-TRUNCATION INTEGRATORS FOR EVOLUTION EQUATIONS ON LOW-RANK TENSOR MANIFOLDS*

ABRAM RODGERS[†] AND DANIELE VENTURI[‡]

Abstract. We develop a new class of algorithms, which we call step-truncation methods, to integrate in time an initial value problem for an ODE or a PDE on a low-rank tensor manifold. The new methods are based on performing a time step with a conventional time-stepping scheme followed by a truncation operation into a tensor manifold with prescribed rank. By considering such truncation operation as a nonlinear operator in the space of tensors, we prove various consistency results and errors estimates for a wide range of step-truncation algorithms. In particular, we establish consistency between the best step-truncation method and the best tangent space projection integrator via perturbation analysis. Numerical applications are presented and discussed for a Fokker–Planck equation on a torus of dimension two and four.

Key words. Hierarchical Tucker tensors; High-dimensional time-dependent PDEs; Low-rank tensor manifolds; Dynamical tensor approximation.

AMS subject classifications. 15A69, 65M22, 35Q84, 65M15.

1. Introduction. Computing the solution of high-dimensional partial differential equations (PDEs) has become central to many new areas of application such as optimal mass transport [13, 48], random dynamical systems [21, 46, 47], mean field optimal control [11, 38], and functional-differential equations [45, 44]. Classical numerical methods based on full tensor product discretizations are not viable in practice, due to the exponential growth of the degrees of freedom with the dimension. To address this problem, a significant research effort has been recently focused on developing effective approximation methods for high-dimensional PDEs. In particular, techniques such as sparse collocation [5, 7, 3, 12, 32], physics-informed neural networks [30, 33, 34, 49] and tensor methods [20, 2, 36, 4, 16, 24] were proposed to mitigate the exponential growth in complexity [40], computational cost and memory requirements.

To describe the mathematical setting, let us consider the following initial value problem for an abstract nonlinear evolution equation

$$(1.1) \quad \frac{\partial f(t, \mathbf{x})}{\partial t} = \mathcal{N}(f(t, \mathbf{x}), \mathbf{x}), \quad f(0, \mathbf{x}) = f_0(\mathbf{x}),$$

where $f : [0, T] \times \Omega \mapsto \mathbb{R}$ is a d -dimensional (time-dependent) scalar field defined in the domain $\Omega \subseteq \mathbb{R}^d$ ($d \geq 2$), and \mathcal{N} is a nonlinear operator which may be dependent on \mathbf{x} and may incorporate boundary conditions. Equation (1.1) is first approximated with respect to the variables $\mathbf{x} = (x_1, \dots, x_d)$, e.g., by finite differences [42] or pseudo-spectral methods [17]. If $f(t, \mathbf{x})$ is an element of a separable Hilbert space $H(\Omega)$ for all $t \geq 0$, then (1.1) can be transformed into the following system of ordinary differential equations

$$(1.2) \quad \frac{d\mathbf{f}(t)}{dt} = \mathbf{N}(\mathbf{f}(t)), \quad \mathbf{f}(0) = \mathbf{f}_0,$$

where $\mathbf{f} : [0, T] \rightarrow \mathbb{R}^{n_1 \times n_2 \times \dots \times n_d}$ is multi-dimensional array of real numbers (the solution tensor), and \mathbf{N} is a tensor-valued nonlinear map (the discrete form of \mathcal{N}). The structure of \mathbf{N} depends on the discretization scheme, as well as on the tensor format utilized for \mathbf{f} . Combining (1.2) with an ODE formula for the time-stepping, e.g., the Adams-Bashforth formula, yields a fully discrete system of nonlinear equations. For instance, if we discretize (1.2) in time with a one-step method on an evenly-spaced grid we obtain

$$(1.3) \quad \mathbf{f}_{k+1} = \mathbf{f}_k + \Delta t \Phi(\mathbf{N}, \mathbf{f}_k, \Delta t),$$

where $\mathbf{f}_k = \mathbf{f}(k\Delta t)$ for $k = 0, 1, \dots$, etc. Of particular interest are low-rank tensor approximations of the solution to (1.2). Such approximations allow us to significantly reduce the number of degrees of freedom in the representation of the solution tensor $\mathbf{f}(t)$, while maintaining accuracy. Low-rank tensor approximations

*
Funding: This research was supported by the U.S. Army Research Office grant W911NF1810309, and by the U.S. Air Force Office of Scientific Research grant FA9550-20-1-0174.

[†]Department of Applied Mathematics, University of California Santa Cruz, Santa Cruz (CA) 95064 (akrodger@ucsc.edu)

[‡]Department of Applied Mathematics, University of California Santa Cruz, Santa Cruz (CA) 95064 (venturi@ucsc.edu)

of (1.2) can be constructed by using, e.g., rank-constrained temporal integration [28, 23, 10, 9] on a smooth Euclidean tensor manifold with constant rank [43, 18].

Alternatively, one can utilize the fully discrete scheme (1.3) followed by a rank-reduction (truncation) operation [14, 15, 25]. These methods will be called *step-truncation methods* [36], and their analysis is one of the main objectives of the present paper. With reference to the time stepping scheme (1.3), a step-truncation method can be written as

$$(1.4) \quad \mathbf{f}_{k+1} = \mathfrak{T}_{\mathbf{r}}(\mathbf{f}_k + \Delta t \Phi(\mathbf{N}, \mathbf{f}_k, \Delta t)),$$

where $\mathfrak{T}_{\mathbf{r}}(\cdot)$ is a tensor rank reduction operation, i.e., a nonlinear projection to a tensor manifold with multilinear rank \mathbf{r} [43]. The need for tensor rank-reduction when integrating (1.2) in time with (1.3) can be easily understood by noting that additions between tensors and the application of an operator to a tensor increase the tensor rank [25]. Hence, iterating (1.3) in the space of tensors with no rank reduction can yield a fast growth of the tensor rank which, in turn, can tax the memory requirements and the computational cost significantly, especially in high dimensions. To thoroughly analyze the step-truncation algorithms we propose in this paper, we will leverage the operator framework we recently introduced in [36], where a projection onto a low-rank tensor manifold is seen as a nonlinear operator in the space of tensors. This allows us to prove various consistency results and errors estimates for a wide range of step-truncation methods. In particular, we establish consistency between the best step-truncation method and the best tangent space projection integrator proposed by Lubich *et al.* in [28, 23, 27].

This paper is organized as follows. In section 2 we introduce three distinct time integrators, namely the best step-truncation (B-ST) integrator, the SVD step-truncation (SVD-ST) integrator, and the best tangent space projection (B-TSP) integrator, to solve (1.2) on a tensor manifold with fixed rank. In section 3 and section 4 we develop a thorough analysis of B-ST and SVD-ST, respectively. In particular, we prove that B-ST is consistent with B-TSP as the time step Δt goes to zero. In section 5 we obtain necessary and sufficient conditions for B-ST and SVD-ST to be high-order integrators. Numerical examples demonstrating the theoretical claims are presented and discussed in section 6. The main findings are summarized in section 7. We also include two brief appendices in which we develop a perturbation analysis of B-ST in two dimensions (Appendix A), and summarize the parallel implementation of the hierarchical Tucker tensor format we utilized for our numerical simulations (Appendix B).

2. Temporal integrators on tensor manifolds with fixed rank. Let $\mathcal{H}_{\mathbf{r}} \subseteq \mathbb{R}^{n_1 \times n_2 \times \dots \times n_d}$ be the manifold of hierarchical Tucker tensors with rank $\mathbf{r} = \{r_t\}$ corresponding to a prescribed dimension tree $t \in \mathcal{T}_d$ [43]. We are interested in developing consistent algorithms for computing the approximate solution of (1.2) in $\overline{\mathcal{H}_{\mathbf{r}}}$ (closure¹ of $\mathcal{H}_{\mathbf{r}}$). To this end, we begin by presenting three different nonlinear projections onto $\overline{\mathcal{H}_{\mathbf{r}}}$ which are fundamental to the development of step-truncation algorithms. The first is the so-called “best approximation” as described by Grasedyck in [14], and it is defined by the minimization principle

$$(2.1) \quad \mathfrak{T}_{\mathbf{r}}^{best}(\mathbf{f}) = \underset{\mathbf{h} \in \overline{\mathcal{H}_{\mathbf{r}}}}{\operatorname{argmin}} \|\mathbf{f} - \mathbf{h}\|_2.$$

The second projector is known as high-order singular value decomposition [15] (HOSVD, or more concisely SVD). Such projector is defined as composition of linear projections obtained from a sequence of singular value decompositions of appropriate matricizations of the tensor \mathbf{f} . These projections are denoted in terms of the layers $\mathcal{T}_d^1 \dots \mathcal{T}_d^p$ of the dimension tree

$$(2.2) \quad \mathfrak{T}_{\mathbf{r}}^{SVD}(\mathbf{f}) = \prod_{t \in \mathcal{T}_d^p} \mathbf{P}_t \cdots \prod_{t \in \mathcal{T}_d^1} \mathbf{P}_t \mathbf{f}.$$

When applied to linear multistep integration schemes this projector is proved to yield a stable method [36]. The third projector we consider is the best projector onto tangent space of $\mathcal{H}_{\mathbf{r}}$. This projector takes a vector $\mathbf{v} \in \mathbb{R}^{n_1 \times n_2 \times \dots \times n_d}$ and projects it onto the tangent space of $\mathcal{H}_{\mathbf{r}}$ at some point $\mathbf{f} \in \mathcal{H}_{\mathbf{r}}$, i.e.

$$(2.3) \quad \mathcal{P}_{\mathbf{f}} \mathbf{v} = \underset{\mathbf{h} \in T_{\mathbf{f}} \mathcal{H}_{\mathbf{r}}}{\operatorname{argmin}} \|\mathbf{v} - \mathbf{h}\|_2,$$

¹ It was shown in [43] that $\overline{\mathcal{H}_{\mathbf{r}}}$ is the set of hierarchical Tucker tensors with ranks at most \mathbf{r} .

where $T_{\bar{\mathbf{f}}}\mathcal{H}_{\mathbf{r}}$ denotes the tangent space of $\mathcal{H}_{\mathbf{r}}$ at $\bar{\mathbf{f}}$. In all cases, the norm used is the standard 2-norm in the embedding space. This implies that the projection defined in (2.3) is a linear function of \mathbf{v} , since it is the solution to a linearly constrained least squares problem. Let

$$(2.4) \quad \mathbf{f}_{k+1} = \mathbf{f}_k + \Delta t_k \Phi(\mathbf{N}, \mathbf{f}_k, \Delta t_k)$$

be a convergent one-step scheme² approximating the solution to the initial value problem (1.2). For example, the Heun method (explicit RK2) can be written in the form (2.4) provided we define

$$(2.5) \quad \Phi(\mathbf{N}, \mathbf{f}_k, \Delta t_k) = \frac{1}{2} [\mathbf{N}(\mathbf{f}_k) + \mathbf{N}(\mathbf{f}_k + \Delta t_k \mathbf{N}(\mathbf{f}_k))].$$

Given $\mathbf{f}_k \in \bar{\mathcal{H}}_{\mathbf{r}}$ we have no guarantee that \mathbf{f}_{k+1} defined in (2.4) is still in $\bar{\mathcal{H}}_{\mathbf{r}}$. To make sure that this is the case, we can apply the nonlinear projection (2.1) or (2.2) to the right hand side of (2.4). This yields the following *step-truncation* methods:

$$(2.6) \quad \mathbf{f}_{k+1} = \mathfrak{T}_{\mathbf{r}}^{best}(\mathbf{f}_k + \Delta t_k \Phi(\mathbf{N}, \mathbf{f}_k, \Delta t_k)).$$

$$(2.7) \quad \mathbf{f}_{k+1} = \mathfrak{T}_{\mathbf{r}}^{SVD}(\mathbf{f}_k + \Delta t_k \Phi(\mathbf{N}, \mathbf{f}_k, \Delta t_k)),$$

Both methods aim at solving (1.2) in $\bar{\mathcal{H}}_{\mathbf{r}}$ by performing a nonlinear projection onto $\bar{\mathcal{H}}_{\mathbf{r}}$ at each time step. In applications, we will refer to them as the best step-truncation (B-ST) and the SVD step-truncation (SVD-ST) methods, respectively.

An alternative method which leads to a differential equation on a tensor manifold with a given rank (i.e., $\mathcal{H}_{\mathbf{r}}$) was developed in [28] (see also [27, 22, 23]). The differential equation follows from the variational principle (2.3), with \mathbf{v} replaced by $\mathbf{N}(\bar{\mathbf{f}})$, and it can be written as

$$(2.8) \quad \frac{d\bar{\mathbf{f}}}{dt} = \mathcal{P}_{\bar{\mathbf{f}}}\mathbf{N}(\bar{\mathbf{f}}),$$

where $\mathcal{P}_{\bar{\mathbf{f}}}$ is the projection (2.3) onto the tangent space of $\mathcal{H}_{\mathbf{r}}$ at $\bar{\mathbf{f}}$. Since this method also comes from a minimization principle, we shall refer to it as the best tangent space projection (B-TSP) method. A temporal discretization of (2.8) with the one-step method (2.4) yields

$$(2.9) \quad \bar{\mathbf{f}}_{k+1} = \bar{\mathbf{f}}_k + \Delta t_k \Phi(\mathcal{P}_{\bar{\mathbf{f}}}\mathbf{N}, \bar{\mathbf{f}}_k, \Delta t_k).$$

Our goal in the following sections is to relate methods (2.6), (2.7) and (2.9) from the perspective of consistency and local error analysis.

3. Analysis of the best step-truncation integrator. Here we show that the best step-truncation scheme (2.6) is consistent with (2.9) at least to order one in Δt , as Δt goes to zero. To this end, we first notice that while $\mathfrak{T}_{\mathbf{r}}^{best}$ gives an element in the closure of $\mathcal{H}_{\mathbf{r}}$, the tangent projector $\mathcal{P}_{\bar{\mathbf{f}}}$ is defined in terms of a given element \mathbf{f} on the interior. To circumvent this issue we resort to a perturbation analysis of the best step-truncation operator, i.e., a formal power series expansion of the form

$$(3.1) \quad \mathfrak{T}_{\mathbf{r}}^{best}(\mathbf{f}_k + \varepsilon \mathbf{v}) = \mathfrak{T}_{\mathbf{r}}^{best}(\mathbf{f}_k) + \varepsilon \frac{\partial \mathfrak{T}_{\mathbf{r}}^{best}(\mathbf{f}_k)}{\partial \mathbf{f}} \mathbf{v} + \dots,$$

where $\partial \mathfrak{T}_{\mathbf{r}}^{best}(\mathbf{f}_k)/\partial \mathbf{f}$ denotes the Jacobian of $\mathfrak{T}_{\mathbf{r}}^{best}$ at $\mathbf{f}_k \in \mathcal{H}_{\mathbf{r}}$, and $\varepsilon \mathbf{v} \in \mathbb{R}^{n_1 \times n_2 \times \dots \times n_d}$. Since $\mathbf{f}_k \in \mathcal{H}_{\mathbf{r}}$, we have that $\mathfrak{T}_{\mathbf{r}}^{best}(\mathbf{f}_k) = \mathbf{f}_k$. This allows us to write (3.1) as

$$(3.2) \quad \mathfrak{T}_{\mathbf{r}}^{best}(\mathbf{f}_k + \varepsilon \mathbf{v}) = \mathbf{f}_k + \varepsilon \frac{\partial \mathfrak{T}_{\mathbf{r}}^{best}(\mathbf{f}_k)}{\partial \mathbf{f}} \mathbf{v} + \dots,$$

The following Proposition characterizes the Jacobian $\partial \mathfrak{T}_{\mathbf{r}}^{best}(\mathbf{f})/\partial \mathbf{f}$ as a continuous function of \mathbf{f} in $\mathcal{H}_{\mathbf{r}}$, and shows that it coincides with the projection operator (2.3) onto the tangent space $T_{\bar{\mathbf{f}}}\mathcal{H}_{\mathbf{r}}$.

² As is well-known, the scheme (2.4) includes Runge-Kutta and also linear multi-step methods. In the latter case the vector \mathbf{f}_k is defined by stacking the solution at different time steps, while \mathbf{N} need to be modified accordingly (see [36] for details).

PROPOSITION 3.1 (Smoothness of the best truncation operator). $\mathfrak{T}_{\mathbf{r}}^{best}(\mathbf{f})$ is continuously differentiable in $\mathcal{H}_{\mathbf{r}}$. Moreover,

$$(3.3) \quad \frac{\partial \mathfrak{T}_{\mathbf{r}}^{best}(\mathbf{f})}{\partial \mathbf{f}} = \mathcal{P}_{\mathbf{f}} \quad \forall \mathbf{f} \in \mathcal{H}_{\mathbf{r}}$$

where $\mathcal{P}_{\mathbf{f}}$ is the projection (2.3) onto the tangent space of $\mathcal{H}_{\mathbf{r}}$ at \mathbf{f} .

Remark 3.2. As discussed in [14], every tensor has an exact hierarchical Tucker (HT) decomposition. From [43], we also know that every HT decomposition lies in some closure $\overline{\mathcal{H}_{\mathbf{r}}}$. Moreover, we know that the boundary of $\overline{\mathcal{H}_{\mathbf{r}}}$ is a union of lower rank open (interior) manifolds. Thus, every point in $\mathbb{R}^{n_1 \times n_2 \times \dots \times n_d}$ is either the tensor of zeros everywhere or exists as an element of a fixed rank manifold. So we have that Proposition 3.1 applies everywhere but the origin.

To prove Proposition 3.1 we first need to ensure that the topology of $\mathcal{H}_{\mathbf{r}}$ is nice enough so as to guarantee that the Jacobian of $\mathfrak{T}_{\mathbf{r}}^{best}$ exists everywhere in $\mathcal{H}_{\mathbf{r}}$. For this, we have the following

LEMMA 3.3. Let $\mathbf{f} \in \mathcal{H}_{\mathbf{r}}$ be a point on the hierarchical Tucker manifold of constant rank. Let $\mathbf{v} \in T_{\mathbf{f}}\mathcal{H}_{\mathbf{r}}$ be an arbitrary vector in the tangent plane of $\mathcal{H}_{\mathbf{r}}$ at \mathbf{f} . Then there exists $\eta > 0$ so that for all ε satisfying $0 \leq \varepsilon \leq \eta$, we have $\mathbf{f} + \varepsilon \mathbf{v} = \mathbf{g} \in \mathcal{H}_{\mathbf{r}}$. As a consequence, if $U_{\mathbf{f}} \subseteq T_{\mathbf{f}}\mathcal{H}_{\mathbf{r}}$ is a closed and bounded set containing the origin, then there exists an open subset $V_{\mathbf{f}} \subseteq U_{\mathbf{f}}$ so that $\mathbf{f} + \mathbf{h} \in \mathcal{H}_{\mathbf{r}}$, for all $\mathbf{h} \in V_{\mathbf{f}}$.

Proof. First, consider a simpler problem, where we have two matrices $\mathbf{A}, \mathbf{B} \in \mathbb{R}^{n \times m}$ where \mathbf{A} is full column rank. Consider the function

$$(3.4) \quad p(\eta) = \det((\mathbf{A} + \eta \mathbf{B})^T (\mathbf{A} + \eta \mathbf{B})).$$

Clearly, $p(\eta)$ is a polynomial and thus smooth in η . Moreover, $p(0) \neq 0$ since \mathbf{A} is full column rank. Since p is smooth, there exists some $\eta > 0$ such that $p(\varepsilon) \neq 0$ for all $\varepsilon \in [0, \eta]$. Since the full-rank hierarchical Tucker manifold is defined via the full column rank constraints on an array of matrices corresponding to matricizations of the tensor [43], we can apply the principle above to every full column rank matrix associated with the tree, using addition of a point and a tangent as referenced in Proposition 3 of [8]. We have now proved the part one of the lemma where η is taken to be the minimum over the tree nodes. As for existence of an open set, suppose $U_{\mathbf{f}}$ is bounded. Now we apply the above matrix case to the boundary $\partial U_{\mathbf{f}}$, giving us a star shaped set $S_{\mathbf{f}} \subseteq U_{\mathbf{f}}$. Letting $V_{\mathbf{f}} = S_{\mathbf{f}} \setminus \partial S_{\mathbf{f}}$ be the interior, completes the proof of the lemma. \square

At this point we have all elements to prove Proposition 3.1. Our proof is an adapted version of a general theorem for surfaces without boundary by Marz and Macdonald [29].

Proof. (Proposition 3.1) Let $\mathbf{f} \in \mathcal{H}_{\mathbf{r}} \subseteq \mathbb{R}^{n_1 \times n_2 \times \dots \times n_d}$. By Lemma 3.3, there exists an open norm-ball $B(\mathbf{f}, \kappa)$ located at \mathbf{f} with radius $\kappa > 0$ so that

$$(3.5) \quad \mathbf{f} + \mathbf{v} \in \mathcal{H}_{\mathbf{r}} \quad \forall \mathbf{v} \in \mathcal{P}_{\mathbf{f}}(B(\mathbf{f}, \kappa)).$$

Let $\mathcal{U}_{\mathbf{f}} = \mathcal{H}_{\mathbf{r}} \cap B(\mathbf{f}, \kappa)$ be a set which is open in the topology of $\mathcal{H}_{\mathbf{r}}$. Also, let $(\mathbf{q}_{\mathbf{f}}, \mathbf{q}_{\mathbf{f}}^{-1}(\mathcal{U}_{\mathbf{f}}))$ be a local parametrization at \mathbf{f} . For the parametrizing coordinates, we take an open subset $\mathbf{q}_{\mathbf{f}}^{-1}(\mathcal{U}_{\mathbf{f}}) = V_{\mathbf{f}} \subseteq T_{\mathbf{f}}\mathcal{H}_{\mathbf{r}}$ of the tangent space embedded in $\mathbb{R}^{n_1 \times n_2 \times \dots \times n_d}$. This means that the parametrization $\mathbf{q}_{\mathbf{f}}$ takes tangent vectors as inputs and maps them into tensors in $\mathcal{H}_{\mathbf{r}}$, i.e.

$$(3.6) \quad \mathbf{q}_{\mathbf{f}} : T_{\mathbf{f}}\mathcal{H}_{\mathbf{r}} \rightarrow \mathcal{H}_{\mathbf{r}}.$$

Moreover, we assume that the coordinates are arranged in column major ordering as a vector. This allows for the Jacobian $\partial \mathbf{q}_{\mathbf{f}} / \partial \mathbf{v}$ to be a basis for the tangent space $T_{\mathbf{f}}\mathcal{H}_{\mathbf{r}}$. Note that $\partial \mathbf{q}_{\mathbf{f}} / \partial \mathbf{v}$ is a $(n_1 n_2 \dots n_d) \times \dim(T_{\mathbf{f}}\mathcal{H}_{\mathbf{r}})$ matrix with real coefficients. Now, let $\mathbf{M}(\mathbf{f})$ be a matrix of column vectors spanning the space orthogonal to $T_{\mathbf{f}}\mathcal{H}_{\mathbf{r}}$ in $\mathbb{R}^{n_1 \times n_2 \times \dots \times n_d}$. Since the two linear spaces are disjoint, we have a local coordinate map for the ball $B(\mathbf{f}, \kappa)$, given by

$$(3.7) \quad \mathbf{C}(\mathbf{v}, \mathbf{g}) = \mathbf{q}_{\mathbf{f}}(\mathbf{v}) + [\mathbf{M}(\mathbf{q}_{\mathbf{f}}(\mathbf{v}))]\mathbf{g},$$

where \mathbf{v} is tangent and \mathbf{g} is normal (both column vectors). By construction,

$$(3.8) \quad \mathfrak{T}_{\mathbf{r}}^{best}(\mathbf{C}(\mathbf{v}, \mathbf{g})) = \mathbf{q}_{\mathbf{f}}(\mathbf{v})$$

which is smooth in both \mathbf{v} and \mathbf{g} . Therefore, we can take the total derivative on the embedded space and apply the chain rule to obtain the Jacobian of $\mathfrak{T}_{\mathbf{r}}^{best}(\mathbf{f})$. Doing so, we have

$$(3.9) \quad \frac{\partial}{\partial(\mathbf{v}, \mathbf{g})} \mathfrak{T}_{\mathbf{r}}^{best}(\mathbf{C}(\mathbf{v}, \mathbf{g})) = \frac{\partial \mathfrak{T}_{\mathbf{r}}^{best}}{\partial \mathbf{C}} \frac{\partial \mathbf{C}}{\partial(\mathbf{v}, \mathbf{g})}$$

$$(3.10) \quad = \frac{\partial \mathfrak{T}_{\mathbf{r}}^{best}}{\partial \mathbf{C}} \left[\frac{\partial \mathbf{q}_{\mathbf{f}}}{\partial \mathbf{v}} + \sum_{i=1}^{n^{\perp}} \frac{\partial \mathbf{M}_i(\mathbf{q}_{\mathbf{f}}(\mathbf{v}))}{\partial \mathbf{v}} g_i \Big| \mathbf{M}(\mathbf{q}_{\mathbf{f}}(\mathbf{v})) \right],$$

where the symbol $[\cdot|\cdot]$ denotes column concatenation of matrices, n^{\perp} is the dimension of the normal space $(T_{\mathbf{f}}\mathcal{H}_{\mathbf{r}})^{\perp}$, \mathbf{M}_i is the i -th column of \mathbf{M} , and g_i is the i -th component of \mathbf{g} . We can take $\mathbf{g} = \mathbf{0}$ since the above expression extends smoothly from the embedding space onto $\mathcal{H}_{\mathbf{r}}$. Hence, the Jacobian of \mathfrak{T}^{best} is the solution to the linear equation

$$(3.11) \quad \frac{\partial \mathfrak{T}_{\mathbf{r}}^{best}}{\partial \mathbf{C}} \left[\frac{\partial \mathbf{q}_{\mathbf{f}}}{\partial \mathbf{v}} \Big| \mathbf{M}(\mathbf{q}_{\mathbf{f}}(\mathbf{v})) \right] = \left[\frac{\partial \gamma_{\mathbf{f}}}{\partial(\delta \mathbf{f})} \Big| \mathbf{0} \right].$$

Since the right factor of the left hand side has a pair of orthogonal blocks, we can write the inverse using the pseudo-inverse of the blocks, i.e.,

$$(3.12) \quad \left[\frac{\partial \mathbf{q}_{\mathbf{f}}}{\partial \mathbf{v}} \Big| \mathbf{M}(\mathbf{q}_{\mathbf{f}}(\mathbf{v})) \right]^{-1} = \begin{bmatrix} \left[\frac{\partial \mathbf{q}_{\mathbf{f}}}{\partial \mathbf{v}} \right]^+ \\ [\mathbf{M}(\mathbf{q}_{\mathbf{f}}(\mathbf{v}))]^+ \end{bmatrix}.$$

The right hand side is the block concatenation of the rows of each pseudo-inverse. Plugging the above expression in (3.11), we find

$$(3.13) \quad \frac{\partial \mathfrak{T}_{\mathbf{r}}^{best}}{\partial \mathbf{C}} = \frac{\partial \mathbf{q}_{\mathbf{f}}}{\partial \mathbf{v}} \left[\frac{\partial \mathbf{q}_{\mathbf{f}}}{\partial \mathbf{v}} \right]^+$$

which is exactly the expression for the orthogonal projector onto the tangent space [28]. This completes the proof. \square

We now discuss how Proposition 3.1 can be used to prove consistency between the best step-truncation algorithm (2.6) and the best tangent space projection integrator (2.9). To this end, let $\Phi(\mathbf{N}, \mathbf{f}, \Delta t_k)$ be an order p increment function and let $\mathbf{f}_k \in \mathcal{H}_{\mathbf{r}}$. By using the perturbation series (3.2) and Proposition 3.1 we can conclude that

$$(3.14) \quad \mathfrak{T}_{\mathbf{r}}^{best}(\mathbf{f}_k + \Delta t_k \Phi(\mathbf{N}, \mathbf{f}_k, \Delta t_k)) = \mathbf{f}_k + \Delta t_k \mathcal{P}_{\mathbf{f}_k} \Phi(\mathbf{N}, \mathbf{f}_k, \Delta t_k) + \dots$$

Therefore the best step-truncation scheme (2.6) is consistent at least to order 1 with the projective integration scheme (2.9). We emphasize that equation (3.14) includes also consistency of step-truncation algorithms in the setting of dynamically biorthogonal equations (DyBO) [6], dynamically orthogonal equations (DO) [39], and double dynamically orthogonal equations (DDO) [22].

LEMMA 3.4 (Consistency of B-TSP). *Let $\bar{\mathbf{f}}$ be a solution to the initial value problem (2.8). Then for a time integration period $[0, T]$ where the fixed rank solution exists, we have*

$$(3.15) \quad \frac{d\bar{\mathbf{f}}}{dt} = \mathbf{N}(\bar{\mathbf{f}}) + \mathbf{e}_{\mathbf{r}},$$

where $\mathbf{e}_{\mathbf{r}} = -\mathbf{N}(\bar{\mathbf{f}}) + \mathcal{P}_{\bar{\mathbf{f}}}\mathbf{N}(\bar{\mathbf{f}})$ is the orthogonal complementary error. Additionally, there is an integration time $[0, t]$ where $\mathbf{e}_{\mathbf{r}}$ can be made arbitrarily small by increasing the rank \mathbf{r} .

Proof. To obtain (3.15), we note that

$$\begin{aligned}\frac{d\bar{\mathbf{f}}}{dt} &= \mathcal{P}_{\bar{\mathbf{f}}}\mathbf{N}(\bar{\mathbf{f}}) \\ &= \mathbf{N}(\bar{\mathbf{f}}) - \mathbf{N}(\bar{\mathbf{f}}) + \mathcal{P}_{\bar{\mathbf{f}}}\mathbf{N}(\bar{\mathbf{f}}) \\ &= \mathbf{N}(\bar{\mathbf{f}}) + e_{\mathbf{r}}.\end{aligned}$$

To show that $e_{\mathbf{r}}$ can be made as small as we like, note that we can make the dimension of the tangent space as large as we like, with larger dimension as a function of the singular values of the hierarchical tensor format for $\bar{\mathbf{f}}$. In particular, in [28, Theorem 5.2] rigorous bounds on $e_{\mathbf{r}}$ were proven in terms of the smoothness of \mathbf{N} and the singular values of a particular solution for sufficiently small t . Such bounds can be used here to conclude that $e_{\mathbf{r}}(t)$ can be made as small as we like with the rank \mathbf{r} . \square

We emphasize that Lemma 3.4 is a generalization of [6, Theorem 3.2]. At this point we have all elements to rigorously state consistency between the best step-truncation algorithm (2.6) and the integration scheme (2.8) based on tangent space projection.

THEOREM 3.5 (Consistency of the best step-truncation integrator). *Let*

$$(3.16) \quad \mathbf{f}_{k+1} = \mathbf{f}_k + \Delta t_k \Phi(\mathbf{N}, \mathbf{f}_k, \Delta t_k)$$

be consistent time stepping scheme for the initial value problem (1.2). Then the best step-truncation scheme

$$(3.17) \quad \mathbf{f}_{k+1} = \mathfrak{T}_{\mathbf{r}}^{best}(\mathbf{f}_k + \Delta t_k \Phi(\mathbf{N}, \mathbf{f}_k, \Delta t_k))$$

converges to the equation $d\bar{\mathbf{f}}/dt = \mathcal{P}_{\bar{\mathbf{f}}}\mathbf{N}(\bar{\mathbf{f}})$ in the limit $\Delta t_k \rightarrow 0$ and for fixed hierarchical rank \mathbf{r} . Consequently, asymptotic error estimates in [28] are shared by the best step-truncation integrator (3.17).

Proof. This is direct consequence of Proposition 3.1 and Proposition 3.4 applied to (3.17). \square

4. Analysis of the SVD step-truncation integrator. Now that we have thoroughly analyzed the best truncation operator $\mathfrak{T}_{\mathbf{r}}^{best}$, we can apply those results to a simpler truncation operator based on high-order singular value decomposition [14], i.e., $\mathfrak{T}_{\mathbf{r}}^{SVD}$. The key property which ties these two truncation operators is a bound on how bad the error of SVD truncation can get, proven in [14],

$$(4.1) \quad \|\mathbf{f} - \mathfrak{T}_{\mathbf{r}}^{best}(\mathbf{f})\|_2 \leq \|\mathbf{f} - \mathfrak{T}_{\mathbf{r}}^{SVD}(\mathbf{f})\|_2 \leq \sqrt{2d-3} \|\mathbf{f} - \mathfrak{T}_{\mathbf{r}}^{best}(\mathbf{f})\|_2,$$

where d is the number of tensor product factors which form the space $\mathbb{R}^{n_1 \times n_2 \times \dots \times n_d}$. In the context the PDE (1.1), d is the dimension of the domain Ω . Equation (4.1) allows us to obtain the an error bound for the SVD step-truncation scheme in terms of the best truncation. We will first show that the error bound of SVD step-truncation integrator is dominated by the error of the best step-truncation integrator.

LEMMA 4.1 (Error bound on the SVD step-truncation integrator). *Let $\mathbf{f}(\tau)$ be the exact solution to equation (1.2) on a time interval $\tau \in [0, t)$, and $\Phi(\mathbf{N}, \mathbf{f}, \Delta t)$ an increment function with order of convergence p . Then we have the following local error estimate for the SVD step-truncation integrator*

$$(4.2) \quad \begin{aligned} \|\mathbf{f}(\tau + \Delta t) - \mathfrak{T}_{\mathbf{r}}^{SVD}(\mathbf{f}(\tau) + \Delta t \Phi(\mathbf{N}, \mathbf{f}(\tau), \Delta t))\|_2 \leq \\ K \left(1 + \sqrt{2d-3}\right) \Delta t^{p+1} + \sqrt{2d-3} \|\mathbf{f}(\tau + \Delta t) - \mathfrak{T}_{\mathbf{r}}^{best}(\mathbf{f}(\tau) + \Delta t \Phi(\mathbf{N}, \mathbf{f}(\tau), \Delta t))\|_2. \end{aligned}$$

Proof. First, we apply triangle inequality to

$$(4.3) \quad \begin{aligned} \|\mathbf{f}(\tau + \Delta t) - \mathfrak{T}_{\mathbf{r}}^{SVD}(\mathbf{f}(\tau) + \Delta t \Phi(\mathbf{N}, \mathbf{f}(\tau), \Delta t))\|_2 \leq \\ \|\mathbf{f}(\tau + \Delta t) - (\mathbf{f}(\tau) + \Delta t \Phi(\mathbf{N}, \mathbf{f}(\tau), \Delta t))\|_2 + \\ \|\mathbf{f}(\tau) + \Delta t \Phi(\mathbf{N}, \mathbf{f}(\tau), \Delta t) - \mathfrak{T}_{\mathbf{r}}^{SVD}(\mathbf{f}(\tau) + \Delta t \Phi(\mathbf{N}, \mathbf{f}(\tau), \Delta t))\|_2. \end{aligned}$$

Since the increment function $\Phi(\mathbf{N}, \mathbf{f}(\tau), \Delta t)$ is, by assumption, of order p we have

$$(4.4) \quad \begin{aligned} \|\mathbf{f}(\tau + \Delta t) - \mathfrak{T}_{\mathbf{r}}^{SVD}(\mathbf{f}(\tau) + \Delta t \Phi(\mathbf{N}, \mathbf{f}(\tau), \Delta t))\|_2 \leq \\ K \Delta t^{p+1} + \|\mathbf{f}(\tau) + \Delta t \Phi(\mathbf{N}, \mathbf{f}(\tau), \Delta t) - \mathfrak{T}_{\mathbf{r}}^{SVD}(\mathbf{f}(\tau) + \Delta t \Phi(\mathbf{N}, \mathbf{f}(\tau), \Delta t))\|_2. \end{aligned}$$

Next, we apply (4.1) to obtain

$$(4.5) \quad \begin{aligned} & \|\mathbf{f}(\tau + \Delta t) - \mathfrak{T}_{\mathbf{r}}^{SVD}(\mathbf{f}(\tau) + \Delta t \Phi(\mathbf{N}, \mathbf{f}(\tau), \Delta t))\|_2 \leq \\ & K \Delta t^{p+1} + \left(\sqrt{2d-3}\right) \|\mathbf{f}(\tau) + \Delta t \Phi(\mathbf{N}, \mathbf{f}(\tau), \Delta t) - \mathfrak{T}_{\mathbf{r}}^{best}(\mathbf{f}(\tau) + \Delta t \Phi(\mathbf{N}, \mathbf{f}(\tau), \Delta t))\|_2. \end{aligned}$$

Another application of the triangle inequality yields

$$(4.6) \quad \begin{aligned} & \|\mathbf{f}(\tau + \Delta t) - \mathfrak{T}_{\mathbf{r}}^{SVD}(\mathbf{f}(\tau) + \Delta t \Phi(\mathbf{N}, \mathbf{f}(\tau), \Delta t))\|_2 \leq \\ & K \Delta t^{p+1} + \left(\sqrt{2d-3}\right) \left(\|\mathbf{f}(\tau) + \Delta t \Phi(\mathbf{N}, \mathbf{f}(\tau), \Delta t) - \mathbf{f}(\tau + \Delta t)\|_2 + \right. \\ (4.7) \quad & \left. \|\mathbf{f}(\tau + \Delta t) - \mathfrak{T}_{\mathbf{r}}^{best}(\mathbf{f}(\tau) + \Delta t \Phi(\mathbf{N}, \mathbf{f}(\tau), \Delta t))\|_2 \right). \end{aligned}$$

Collecting like terms yields the desired result. \square

The next Corollary shows that for fixed dimension d , the SVD step-truncation integrator is consistent with the ODE (1.2) as the rank is increased.

COROLLARY 4.2 (Consistency of the SVD step-truncation integrator). *Let Φ and \mathbf{N} be as in Theorem 3.5. Assuming that the error of the best step-truncation integrator can be made arbitrarily small with the rank, we have that the scheme*

$$(4.8) \quad \mathbf{f}_{k+1} = \mathfrak{T}_{\mathbf{r}}^{SVD}(\mathbf{f}_k + \Delta t_k \Phi(\mathbf{N}, \mathbf{f}_k, \Delta t_k))$$

is consistent with (1.2) for fixed d and for increasing rank.

Proof. The Corollary follows immediately from the inequality (4.2), which implies that implies that the SVD truncation error can be made arbitrarily small if the best truncation error can be made arbitrarily small. \square

The following Corollary characterizes an error bound on the SVD step-truncation integrator which depends on the projection onto the tangent space of the tensor manifold $\mathcal{H}_{\mathbf{r}}$. More precisely, by applying series expansion (3.14) to the result (4.2), we can construct another bound for the SVD step-truncation integrator that holds as Δt is taken down to zero. We omit the proof of this corollary, as it essentially follows the same strategy we used in the proof of Lemma 4.1.

COROLLARY 4.3 (Bound on SVD-ST depending on the tangent space projection). *Let Φ and \mathbf{N} be as in Theorem 3.5. Then as $\Delta t \rightarrow 0$ we have*

$$(4.9) \quad \begin{aligned} & \|\mathbf{f}(\tau + \Delta t) - \mathfrak{T}_{\mathbf{r}}^{SVD}(\mathbf{f}(\tau) + \Delta t \Phi(\mathbf{N}, \mathbf{f}(\tau), \Delta t))\|_2 \leq \\ & \sqrt{2d-3} \|\mathbf{f}(\tau + \Delta t) - \mathbf{f}(\tau) - \Delta t \mathcal{P}_{\mathbf{f}(\tau)} \Phi(\mathbf{N}, \mathbf{f}(\tau), \Delta t)\|_2 + M \left(1 + \sqrt{2d-3}\right) \Delta t^2, \end{aligned}$$

where $M > 0$ is obtained from combining the series expansion (3.14) and the scaling coefficients of (4.1).

5. High-order step-truncation integrators. Now that we have given consistency results and error estimates for both B-ST and SVD-ST integrators, we are interested in how accurate of an estimate in time the best truncation method is for the original dynamics (1.2). We see from (3.14) that if the higher order derivatives of $\mathfrak{T}_{\mathbf{r}}^{best}$ are not sufficiently small, then the overall order may be only 1. Hereafter we present a condition on \mathbf{N} for the order of accuracy to (2.8) to be equal to the order of $\Phi(\mathbf{N}, \mathbf{f}, \Delta t)$. Subsequently, we transplant the error bounds obtained in this way to the SVD step-truncation integrator.

PROPOSITION 5.1 (High-order B-ST integrator). *Let*

$$(5.1) \quad \mathbf{f}_{k+1} = \mathbf{f}_k + \Delta t_k \Phi(\mathbf{N}, \mathbf{f}_k, \Delta t_k)$$

be any order p convergent numerical scheme approximating the solution to (1.2). Then $\mathbf{N}(\mathbf{f}) \in T_{\mathbf{f}} \mathcal{H}_{\mathbf{r}}$, i.e. $\mathbf{N}(\mathbf{f}) = \mathcal{P}_{\mathbf{f}} \mathbf{N}(\mathbf{f})$, for a time period $[0, t)$ if and only if

$$(5.2) \quad \mathbf{f}_{k+1} = \mathfrak{T}_{\mathbf{r}}^{best}(\mathbf{f}_k + \Delta t_k \Phi(\mathbf{N}, \mathbf{f}_k, \Delta t_k))$$

is an order p approximation (w.r.t. Δt) of the solution to (1.2).

Proof. First, the forward direction of the proposition. Since $\mathbf{N}(\mathbf{f}) \in T_{\mathbf{f}}\mathcal{H}_{\mathbf{r}}$ we have that $\mathbf{f}(\tau) \in \mathcal{H}_{\mathbf{r}}$ for all $0 \leq \tau < t$. Therefore,

$$(5.3) \quad \|\mathbf{f}(\tau + \Delta t) - (\mathbf{f}(\tau) + \Delta t \Phi(\mathbf{N}, \mathbf{f}_k, \Delta t))\|_2 \leq K \Delta t^{p+1},$$

implies that $\mathfrak{T}_{\mathbf{r}}^{best}(\mathbf{f}_k + \Delta t_k \mathcal{A}_{\Delta t_k}(\mathbf{L}, \mathbf{f}_k))$ is at most $K \Delta t^{p+1}$ away from its argument. Hence, by the triangle inequality, we have

$$\begin{aligned} \|\mathbf{f}(\tau + \Delta t) - \mathfrak{T}_{\mathbf{r}}^{best}(\mathbf{f}(\tau) + \Delta t \Phi(\mathbf{N}, \mathbf{f}(\tau), \Delta t))\|_2 &= \|\mathbf{f}(\tau + \Delta t) - (\mathbf{f}(\tau) + \Delta t \Phi(\mathbf{N}, \mathbf{f}(\tau), \Delta t))\|_2 + \\ &\quad \|\mathbf{f}(\tau) + \Delta t \Phi(\mathbf{N}, \mathbf{f}(\tau), \Delta t) - \\ &\quad \mathfrak{T}_{\mathbf{r}}^{best}(\mathbf{f}(\tau) + \Delta t \Phi(\mathbf{N}, \mathbf{f}(\tau), \Delta t))\|_2 \\ &\leq 2K \Delta t^{p+1}. \end{aligned}$$

Therefore, if $\mathbf{N}(\mathbf{f}) \in T_{\mathbf{f}}\mathcal{H}_{\mathbf{r}}$ then the best step-truncation method retains the order of the scheme (5.1). Now we will prove the converse. Suppose that

$$(5.4) \quad \|\mathbf{f}(\tau + \Delta t) - \mathfrak{T}_{\mathbf{r}}^{best}(\mathbf{f}(\tau) + \Delta t \Phi(\mathbf{N}, \mathbf{f}(\tau), \Delta t))\|_2 \leq K \Delta t^{p+1}.$$

Employing the expansion (3.14), we have

$$\|\mathfrak{T}_{\mathbf{r}}^{best}(\mathbf{f}(\tau) + \Delta t \Phi(\mathbf{N}, \mathbf{f}(\tau), \Delta t)) - (\mathbf{f}(\tau) + \mathcal{P}_{\mathbf{f}(\tau)} \Phi(\mathbf{N}, \mathbf{f}(\tau), \Delta t))\|_2 \leq L \Delta t^2$$

Now we can directly apply the triangle inequality.

$$\begin{aligned} \left\| \frac{\mathbf{f}(\tau + \Delta t) - \mathbf{f}(\tau)}{\Delta t} - \mathcal{P}_{\mathbf{f}(\tau)} \Phi(\mathbf{N}, \mathbf{f}(\tau), \Delta t) \right\|_2 &= \left\| \frac{\mathbf{f}(\tau + \Delta t)}{\Delta t} - \frac{1}{\Delta t} (\mathbf{f}(\tau) + \Delta t \mathcal{P}_{\mathbf{f}(\tau)} \Phi(\mathbf{N}, \mathbf{f}(\tau), \Delta t)) \right\|_2 \\ &\leq \frac{1}{\Delta t} \|\mathbf{f}(\tau + \Delta t) - \mathfrak{T}_{\mathbf{r}}^{best}(\mathbf{f}(\tau) + \Delta t \Phi(\mathbf{N}, \mathbf{f}(\tau), \Delta t))\|_2 \\ &\quad + \frac{1}{\Delta t} \|\mathfrak{T}_{\mathbf{r}}^{best}(\mathbf{f}(\tau) + \Delta t \Phi(\mathbf{N}, \mathbf{f}(\tau), \Delta t)) - (\mathbf{f}(\tau) + \mathcal{P}_{\mathbf{f}(\tau)} \Phi(\mathbf{N}, \mathbf{f}(\tau), \Delta t))\|_2 \\ &\leq K \Delta t^p + L \Delta t \end{aligned}$$

By taking the limit for Δt going to zero we have

$$\|\mathbf{N}(\mathbf{f}(\tau)) - \mathcal{P}_{\mathbf{f}(\tau)} \mathbf{N}(\mathbf{f}(\tau))\|_2 = 0. \quad \square$$

Remark 5.2. Proposition 5.1 suggests that we should expect a high-order of accuracy when applying the discretization scheme (2.9) if the rank of the solution to (1.2) does not change in time. Moreover, the series expansion (3.14) tells us that the order of accuracy of (2.9) is lower bounded by one. Hence, we can conclude that the equation (2.9) has order of accuracy which is dependent on the dynamics defined by (1.2).

We now apply these results to the SVD step-truncation integrator. The following Corollary characterizes the order of accuracy of the scheme (2.7).

COROLLARY 5.3 (High-order SVD step-truncation integrator). *If $\mathbf{N}(\mathbf{f}) \in T_{\mathbf{f}}\mathcal{H}_{\mathbf{r}}$ then the SVD step-truncation integrator*

$$(5.5) \quad \mathbf{f}_{k+1} = \mathfrak{T}_{\mathbf{r}}^{SVD}(\mathbf{f}_k + \Delta t_k \Phi(\mathbf{N}, \mathbf{f}_k), \Delta t_k),$$

has the same order of accuracy (in time) as the scheme (5.1).

Proof. The proof follows immediately by combining Proposition 5.1 and inequality (4.1). Note that the error scaling coefficient is dependent on dimension of the domain. \square

Remark 5.4. Though the best truncation \mathfrak{T}^{best} has some desirable theoretical properties, we remark that it is the solution to a possibly large-scale optimization problem (2.1). Solving such a large problem can be computationally costly. However, many of the desirable features of \mathfrak{T}^{best} are inherited by the SVD truncation operator \mathfrak{T}^{SVD} . Moreover, the SVD truncation has efficient numerical implementations [15, 25].

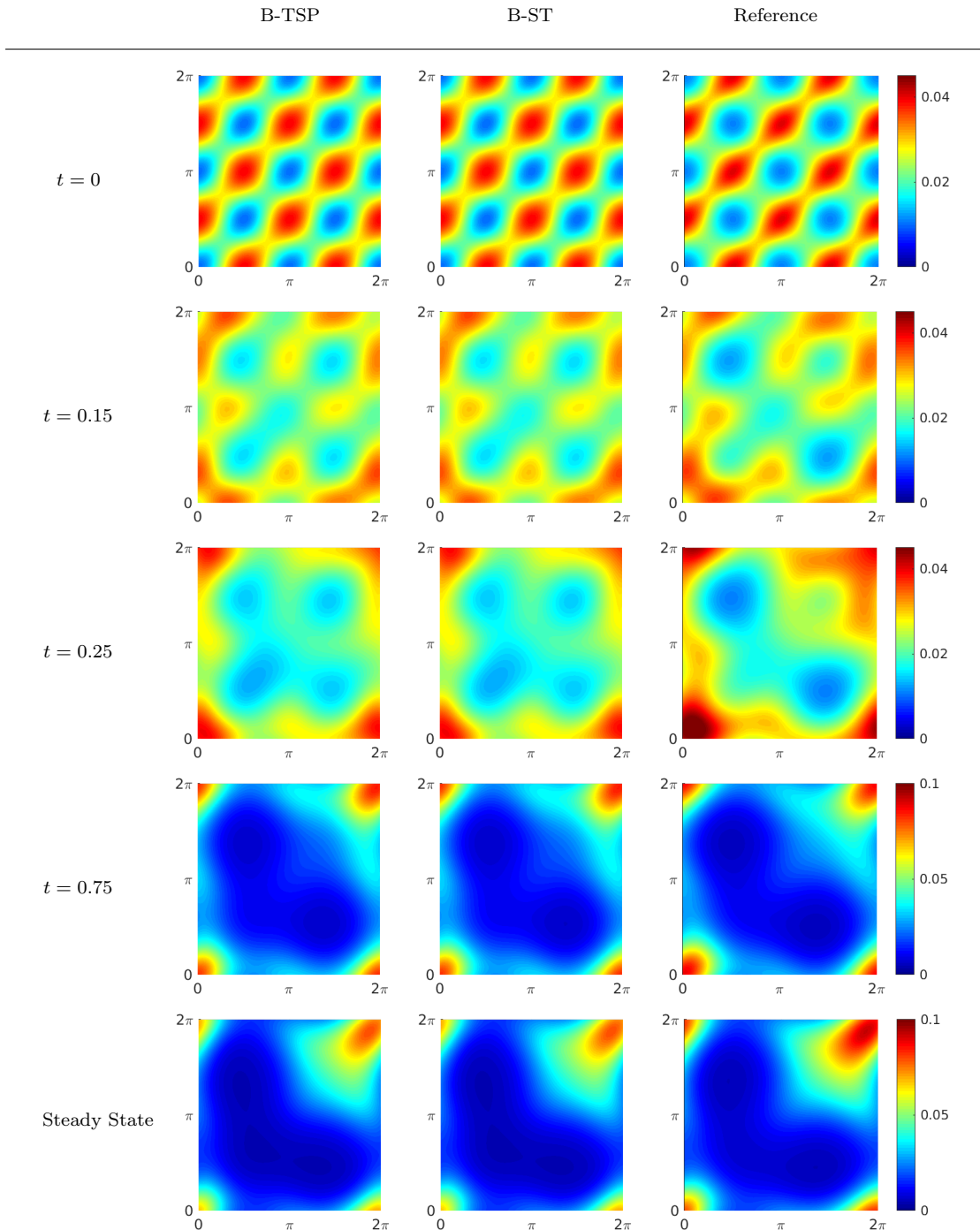


FIG. 1. Numerical solution to the Fokker–Planck equation (6.3) in dimension $d = 2$ obtained with three distinct methods: best tangent space projection (B-TSP) integrator (2.9), best step-truncation (B-ST) integrator (2.6), and full tensor product integrator (2.4) (reference solution). These solutions were computed by discretizing the initial condition (6.4) on an evenly spaced grid with 70×70 interior points, and then truncating the corresponding tensor (matrix) to rank $r = 3$, which is kept constant throughout the simulations. The discretized Fokker–Planck operator is built on the same grid with a Fourier pseudo-spectral expansion. The steady state is determined for this computation by halting execution when $\|\partial f_{ref}/\partial t\|_2$ is below a numerical threshold of 10^{-12} . This happens at approximately $t \simeq 20$ for the initial condition (6.4).

6. An application to the Fokker–Planck equation. In this section we apply the proposed step-truncation algorithms to a Fokker–Planck equation with non-constant drift and constant diffusion coefficients,

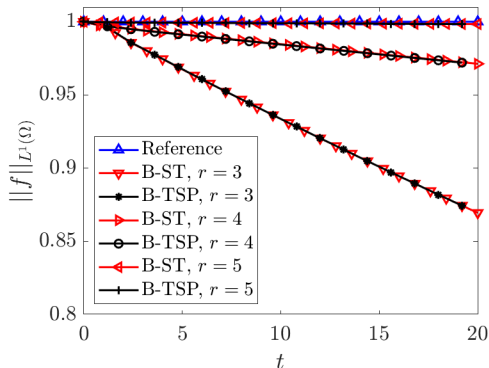


FIG. 2. L_1 norm of the solution to the Fokker–Planck equation (6.3) in dimension $d = 2$. The choice of the initial condition and discretization scheme is the same as in Figure 1.

and demonstrate their accuracy in predicting relaxation to statistical equilibrium. To this end, consider the following stochastic model

$$(6.1) \quad dx_i = \mu_i(\mathbf{x})dt + \sigma dW_i, \quad i = 1, \dots, d$$

where $\sigma = 2$,

$$(6.2) \quad \mu_i(\mathbf{x}) = (\gamma(x_{i+1}) - \gamma(x_{i-2}))\xi(x_{i-1}) - \phi(x_i),$$

$\gamma(x) = \sin(x)$, $\xi(x) = \cos(x)$, and $\phi(x) = \exp(\sin(x)) + 1$. In equation (6.1), (x_1, \dots, x_d) are the phase variables of the model, which we assume periodic (i.e., $x_{i+d} = x_i$), and (W_1, \dots, W_d) is a standard vector-valued Wiener process. The Fokker–Planck equation that corresponds to (6.1) has the form

$$(6.3) \quad \frac{\partial f(\mathbf{x}, t)}{\partial t} = - \sum_{i=1}^d \frac{\partial}{\partial x_i} (\mu_i(\mathbf{x})f(\mathbf{x}, t)) + \frac{\sigma^2}{2} \sum_{i=1}^d \frac{\partial^2 f(\mathbf{x}, t)}{\partial x_i^2}.$$

Our numerical examples will be computed on a torus $\Omega = [0, 2\pi]^d$ with dimension $d = 2$ and $d = 4$.

6.1. Two-dimensional Fokker-Planck equation. In Figure 1 we plot the numerical solution of the Fokker–Planck equation (6.3) in dimension $d = 2$ we obtained with three distinct methods: best tangent space projector (B-TSP) integrator (2.9), best step-truncation (B-ST) integrator (2.6), and full tensor product integrator (2.4) (benchmark solution, hereafter denoted as f_{ref}). These solutions were computed by discretizing the initial condition

$$(6.4) \quad f_0(x_1, x_2) = \frac{1}{m_0} \left[e^{\sin(x_1 - x_2)^2} + \sin(x_1 + x_2)^2 \right],$$

where m_0 is a normalization factor, on a grid with 70×70 evenly-spaced interior points, and then truncating the corresponding tensor (matrix) to rank $r = 3$. The discretized Fokker–Planck operator \mathbf{N} appearing in Eq. (1.2) is built on the same grid with a Fourier pseudo-spectral expansion. The time stepping scheme is a strong stability preserving RK3. This defines the iteration function Φ in the schemes (2.4), (2.6) and (2.9). The steady state was determined for this computation by halting execution when $\|\partial f_{ref}/\partial t\|_2$ was below a numerical threshold of 10^{-12} . This happens at approximately $t \simeq 20$ for the initial condition (6.4). We can see from Figure 1 that even for a fairly small rank ($r = 3$), the best step-truncation method (2.6) and the best tangent space projection integrator (2.9) still capture much of the qualitative behavior of the full state probability density. It is worth noting here that the ability for the various fixed-rank approximations to capture the behavior of an initial value problem is dependent on both initial condition and the dynamical system under consideration.

As is well known, in the two-dimensional setting we are considering in this section (discretized solution in the (x_1, x_2) plane at each time), the best truncation operator \mathfrak{T}_r^{best} coincides with the SVD truncation

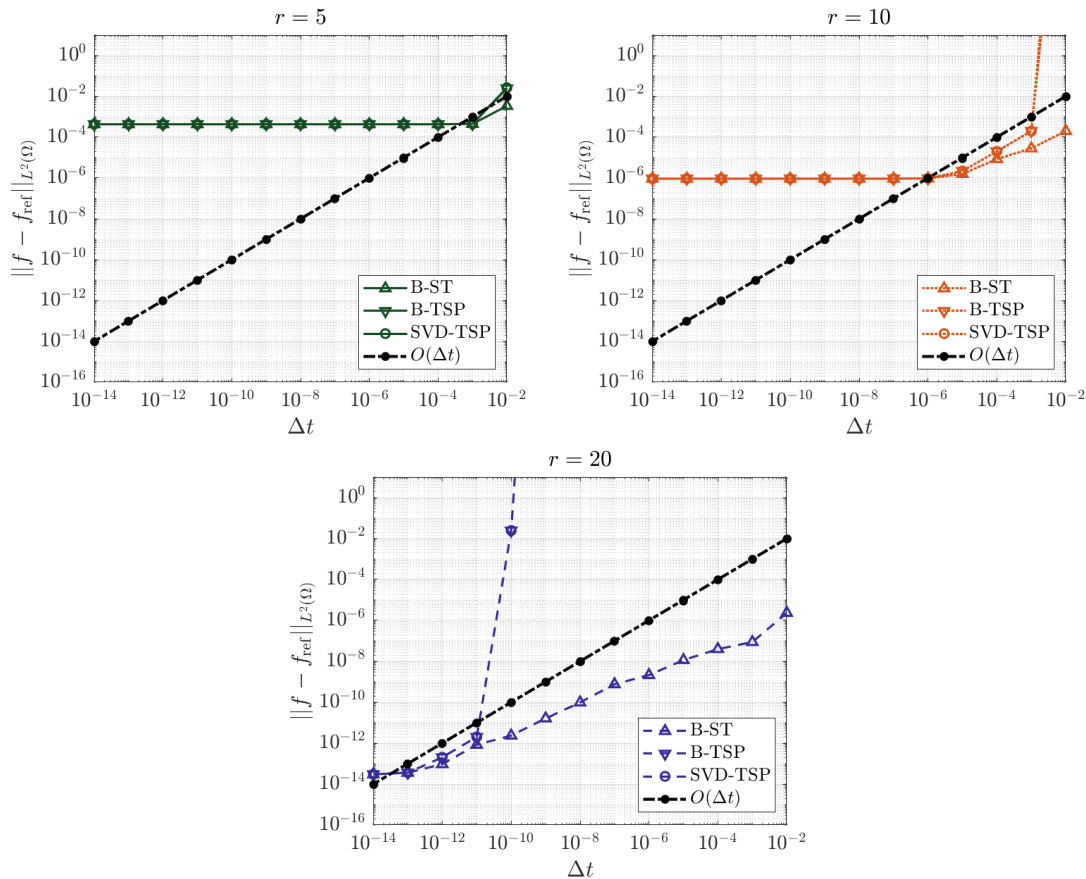


FIG. 3. Local truncation error to the reference solution of the best step-truncation (B-ST) integrator, best tangent space projection (B-TSP) integration (2.8), and perturbed singular value decomposition tangent space projection (SVD-TSP) method (Appendix A) for different ranks r . These plots were constructed by first truncating the initial condition to rank r , and then computing the error corresponding to one time step with each scheme. The error is measured in $L^2([0, 2\pi]^2)$ metric relative to a reference solution obtained with a Fourier Spectral method. The choice of the initial condition and discretization scheme is the same as in Figure 1.

(classical SVD), i.e., we have $\mathfrak{X}_r^{best} = \mathfrak{X}_r^{SVD}$. This allows us to easily provide a numerical verification of Theorem 3.5. The theorem makes two claims. The first claim is that there exists a rank r , and a time step Δt such that the local truncation error can be made smaller than any fixed $\epsilon > 0$. The second claim is that the best step-truncation integrator (2.6) is consistent with the projected tangent space dynamics (2.9) as $\Delta t \rightarrow 0$ on a matrix manifold with fixed rank. That is, if $\bar{\mathbf{f}}(t)$ solves (2.8) then in a neighborhood around the point $\bar{\mathbf{f}}(t) \in \mathcal{H}_r$ we have

$$(6.5) \quad \|\bar{\mathbf{f}}(t + \Delta t) - \mathfrak{X}_r^{best}(\bar{\mathbf{f}}(t) + \Delta t \Phi(\mathbf{N}, \bar{\mathbf{f}}(t), \Delta t))\|_2 \leq K_r \Delta t^{p+1}.$$

Above, we have $p \geq 1$ as the order of consistency and K_r as the error scaling constant determined by the derivatives of \mathfrak{X}_r^{best} . For these numerical examples, we estimate the accuracy by examining the error of a common RK3 scheme. This ensures that the numerical error order is less than the theoretical bound $p \geq 1$.

In Figure 2 we plot the L^1 norm of the solution we obtained with B-ST and B-TSP. Nothing about our analysis implies that for a fixed rank will we see preservation of quantities such as probability mass. It is only the case that as rank is taken sufficiently large do we see proper retaining of those quantities. Numerically speaking, our discrete time integration scheme does not take into account any mass preservation properties which may be upheld before tangent space projection. However, by Theorem 3.17 the error can be made arbitrarily small. Thus we must have preservation in the limiting case. If the initial condition has a high rank with slowly decaying singular values, then as demonstrated in Figure 3 we will have a rather large error penalty from projecting the initial condition into the tensor manifold \mathcal{H}_r . Another interesting

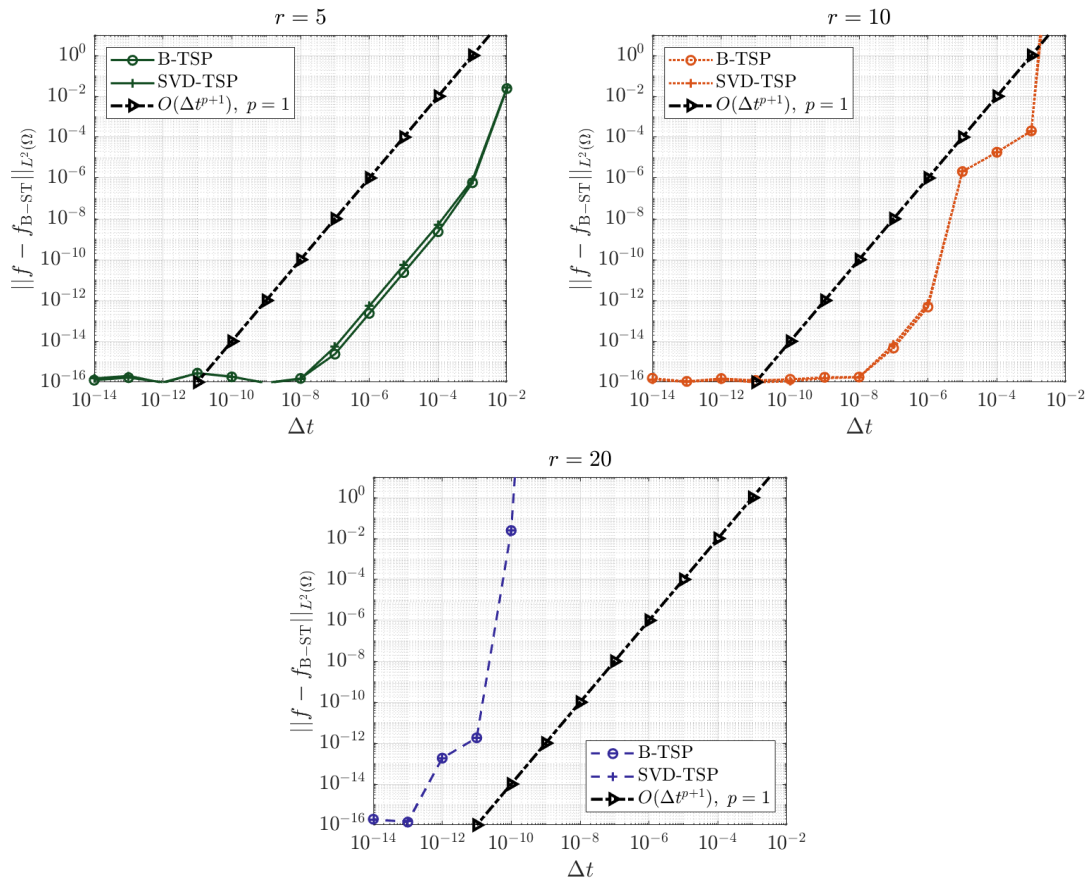


FIG. 4. Local truncation error to best step-truncation integrator of the best tangent space projection (B-TSP) integrator (2.8) and perturbed singular value decomposition tangent space projection (SVD-TSP) method (Appendix A) for different ranks r . As in Figure 3, the plot was made by first truncating the initial condition to rank r , then computing one step under each scheme. The error is measured in $L^2([0, 2\pi]^2)$ norm. The discretization scheme is the same as in Figure 1.

observation from Figure 3 is that the error between the best tangent space projection integrator and the SVD step-truncation method appears to have three characterizing regions. The first region is where the error slope is large and the error is large. This behavior could be explained by Lemma 3.3. In fact, if the perturbation is too large, then we do not guarantee that the numerical update of the solution is within \mathcal{H}_r and therefore the all results we have proved, which hold for small Δt , do not apply. The second error region is one where the slope of the local truncation error is about one in log-log scale. It is our numerical experience that this region begins shortly before a leveling-off in the error due to truncation of the initial condition onto a manifold of lower rank. Interestingly, the best step-truncation integrator does not suffer from these effects. Though, as expected, the asymptotic error for $\Delta t \rightarrow 0$ has the same level for a fixed rank, and is approached rather smoothly. Additionally, we remark that the rate at which the level is approached as $\Delta t \rightarrow 0$ need not be the same for each choice of rank. Our analysis indeed implies that the error can be made arbitrarily small, but does not put any order conditions on the rank. In fact, the rate will be in general dependent on the rank and singular value decay of the initial condition, as well as the full rank dynamics.

In Figure 4 we demonstrate the inequality (6.5) numerically. It is seen that for all the listed ranks that as Δt nears machine accuracy, the order is $p = 1$. This bound holds most clearly for the low rank approximations. We then see that there is the expected cancellation error at machine accuracy of double precision floating point. Again, we see steep slopes for large ranks. This observation combined with Figure 3 gives numerical evidence of some unbearable *stiffness* in the best tangent space projection equation (2.8). In particular, the error constant K_r for large r would seem to be very large. However, a full analysis of the stiffness for these equations is beyond the scope of the present paper.

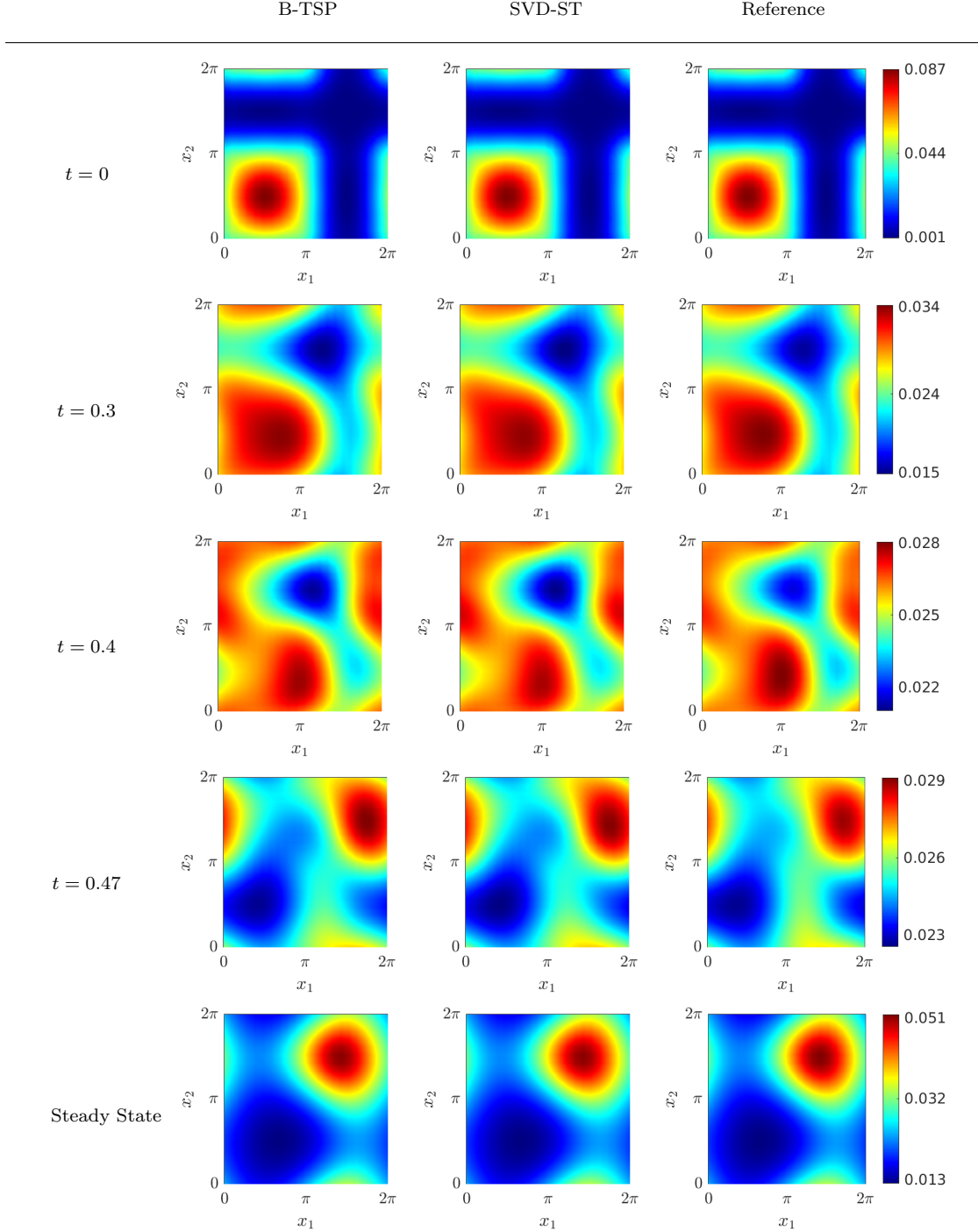


FIG. 5. Numerical solution to the Fokker–Planck equation (6.3) in dimension $d = 4$ obtained with three distinct methods: best tangent space projector (B-TSP) integrator (2.9), SVD step-truncation (SVD-ST) integrator (2.7), and full tensor product integrator (2.4) (reference solution). Specifically, we plot the marginals of the 4-dimensional probability density function $f(x_1, \dots, x_4, t)$ with respect to x_3 and x_4 at different times. These solutions are computed by first truncating the initial condition (6.6) to a hierarchical Tucker balanced tree representation with maximal rank of 5, on a grid with $20 \times 20 \times 20 \times 20$ interior points (evenly spaced). The discretized Fokker–Planck operator is built on the same grid with a Fourier pseudo-spectral expansion. The time stepping scheme is RK1 with $\Delta t = 10^{-4}$. The steady state is determined for this computation by halting execution when $\|\partial f_{ref}/\partial t\|_2$ is below a numerical threshold of 10^{-8} . This happens at approximately $t \approx 6.25$ for the initial condition (6.6).

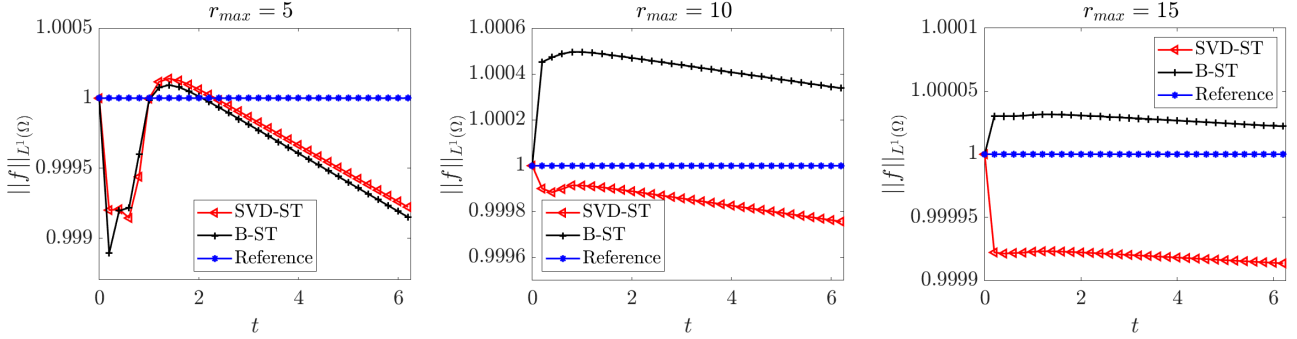


FIG. 6. L_1 norm of the solution to the Fokker–Planck equation (6.3) in dimension $d = 4$. We compare different time-stepping methods: SVD step-truncation (SVD-ST) integrator (2.7), best tangent space projector (B-TSP) integrator (2.9), and full tensor product integrator (Reference) (2.4).

6.2. Four-dimensional Fokker-Planck equation. We now demonstrate numerical results for the Fokker-Planck equation (6.3) in dimension $d = 4$. In this case, the best truncation operator (2.1) is not explicitly known. Instead, we demonstrate numerically various properties of the step-truncation method (2.7), with truncation operator \mathfrak{T}_r^{SVD} defined in [14, 25]. For simplicity, in the following numerical examples, we demonstrate our theory for the simplest possible one-step method, i.e., Euler forward. The initial condition is chosen to be

$$(6.6) \quad f_0(x_1, x_2, x_3, x_4) = \frac{1}{m_0} \sum_{j=1}^M \prod_{i=1}^4 \frac{\sin((2j-1)x_i)}{2^{2(j-1)}} + \prod_{i=1}^4 \frac{\exp(\cos(2jx_i))}{2^{2j-1}},$$

where m_0 is the normalization constant. Clearly, (6.6) can be represented exactly in a hierarchical Tucker tensor format provided we use an overall maximal tree rank of $r_{init} = 2M$. Hereafter, we repeat the numerical tests we presented in section 6.1, but swapping out \mathfrak{T}_r^{best} for \mathfrak{T}_r^{SVD} . For practical purposes of implementation, we will limit our best tangent space projection rank to be at most r_{init} . In Figure 5 we plot a few snapshots of marginal PDF

$$(6.7) \quad f(x_1, x_2, t) = \int_0^{2\pi} \int_0^{2\pi} f(x_1, x_2, x_3, x_4, t) dx_3 dx_4$$

we obtained by integrating (6.3) in time with SVD-ST and B-TSP. As it can be seen from Figure 6 such integrators preserve the L^1 norm of the PDF solution as the multilinear rank \mathbf{r} is increased. In Figure 7 we demonstrate numerically that the inequality (4.9) we obtained in Corollary 4.3 holds true. Note that the simulation setting we consider in this section does not appear to suffer from the same large error we observed in Figure 4 as Δt is increased. Again, this can be justified based on Lemma 3.3. All that needs to be done to provide better accuracy is to pick an initial condition further from the boundary of \mathcal{H}_r . Of course, one does not always have their choice of initial condition. Thus, we have demonstrated both circumstances. Figure 8 demonstrates sub-optimality of the SVD step-truncation integrator (2.7). From the analysis above, we know that \mathfrak{T}_r^{best} and \mathfrak{T}_r^{SVD} are equal on the manifold \mathcal{H}_r . Therefore, if \mathfrak{T}_r^{SVD} had the same Jacobian as \mathfrak{T}_r^{best} we would have that they are equal everywhere. However, this can only be the case if they have the same error to the best tangent space projection integrator for an arbitrary initial value problem. As seen in Figure 8, this is clearly not the case. For our last numerical example, we show that the SVD step-truncation method (2.7) may have an arbitrarily low error to the dynamics without rank constraint. This is observed in Figure 9 for various time steps Δt . Note that these results follow directly from Lemma 4.1 and its Corollary 4.2. We can also get an indication of how much the Fokker–Planck dynamics increases rank in a small time period by observing Figure 9. The initial condition (6.6) was chosen so that $r_{init} = 20$. The dynamics approximately triple this number in a short time. This is due to the combined effect of space-dependent drift and constant diffusion coefficients in (6.3).

7. Summary. In this paper developed a new class of algorithms, which we called step-truncation methods, to integrate in time an initial value problem for an ODE or a PDE on a low-rank tensor manifold. The

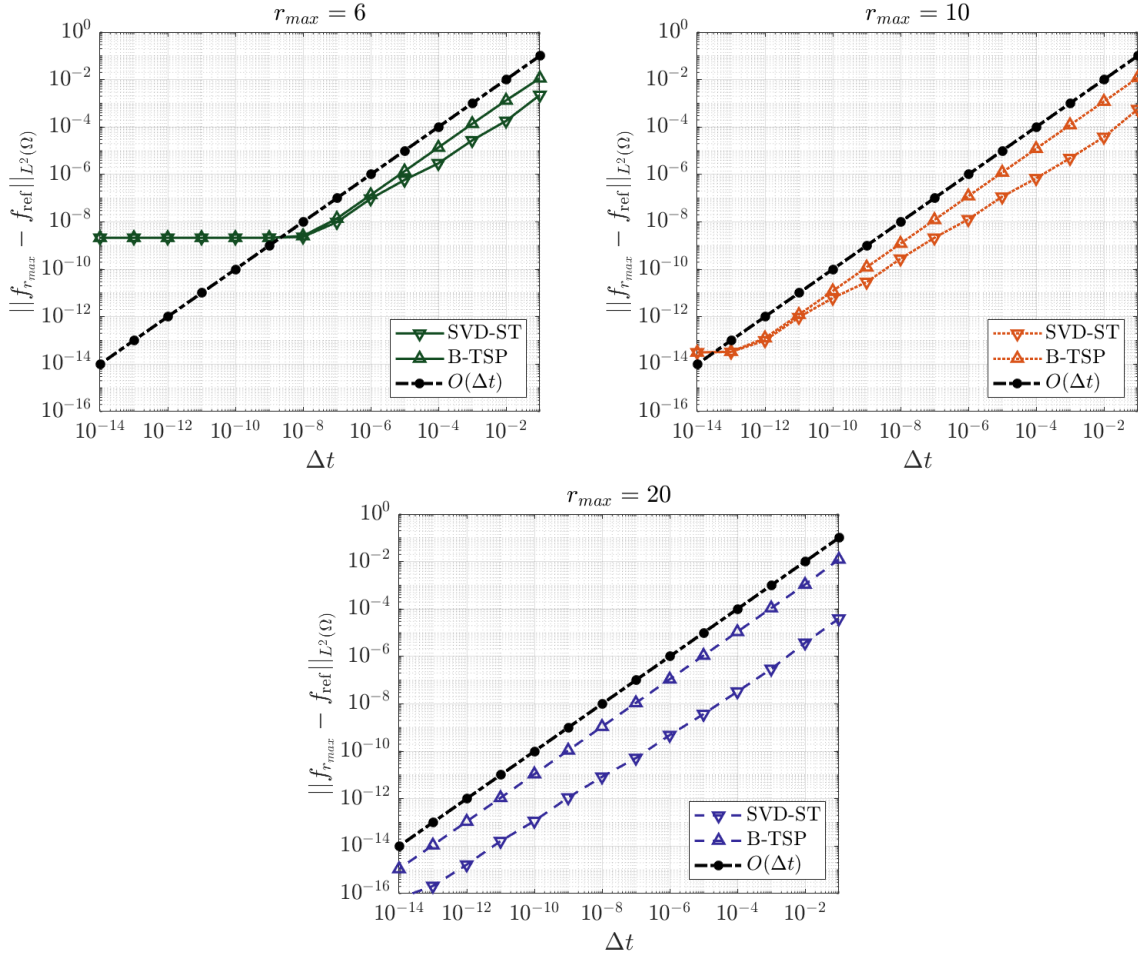


FIG. 7. Numerical demonstration of inequality (4.9). For this example, we chose an initial condition (6.6) with $M = 10$ and a Fourier pseudo-spectral discretization on a grid with $100 \times 100 \times 100 \times 100$ interior points. As above, (SVD-ST) denotes the SVD step-truncation integrator (2.7), while (B-TSP) is the best tangent space projection integrator (2.9). We see that as the maximal rank across all matrices on the dimension tree increases, we have that the SVD step-truncation method has error bounded by $O(\Delta t)$. This is due to the first term in (4.9). In order to achieve a $O(\Delta t^2)$ or better accuracy, we need that term to vanish faster – see Proposition 5.1.

new methods are based on performing a time step with a conventional time-stepping scheme followed by a truncation operation into a hierarchical Tucker tensor manifold with prescribed rank. In particular, we studied step-truncation methods based on best truncation (2.1) and SVD truncation (2.2) operators. We called these methods best step-truncation (B-ST) and SVD step-truncation (SVD-ST) integrators, respectively. By considering the truncation operation as a nonlinear operator in the space of hierarchical Tucker tensors, we proved various consistency results and errors estimates for a wide range of step-truncation methods. In particular, we proved that B-ST is consistent at least to order one with the best tangent space projection (B-TSP) integrator proposed by Lubich *et al.* in [28, 23, 27]. We also provided necessary and sufficient conditions for higher-order consistency. We tested B-ST, SVD-ST and B-TSP on a Fokker–Planck equation with non-constant drift and constant diffusion on a torus in dimension two and four. The numerical results we obtained confirm our theoretical claims and demonstrate that of B-ST and SVD-ST offer computational advantages in terms of ease of implementation, memory requirements, cost and robustness over B-TSP when solving high-dimensional evolution equations.

Appendix A: Perturbation analysis of the best step-truncation integrator. To make Theorem 3.5 concrete, in this Appendix we write down $\mathfrak{T}_{\mathbf{r}}^{best}$ and its Jacobian $\mathcal{P}_{\mathbf{f}}$ for problems where $\mathbf{f} \in \mathbb{R}^{n_1 \times n_2}$ is a matrix. In this situation, the tree rank \mathbf{r} is just a single integer r . One can see from the accuracy inequalities

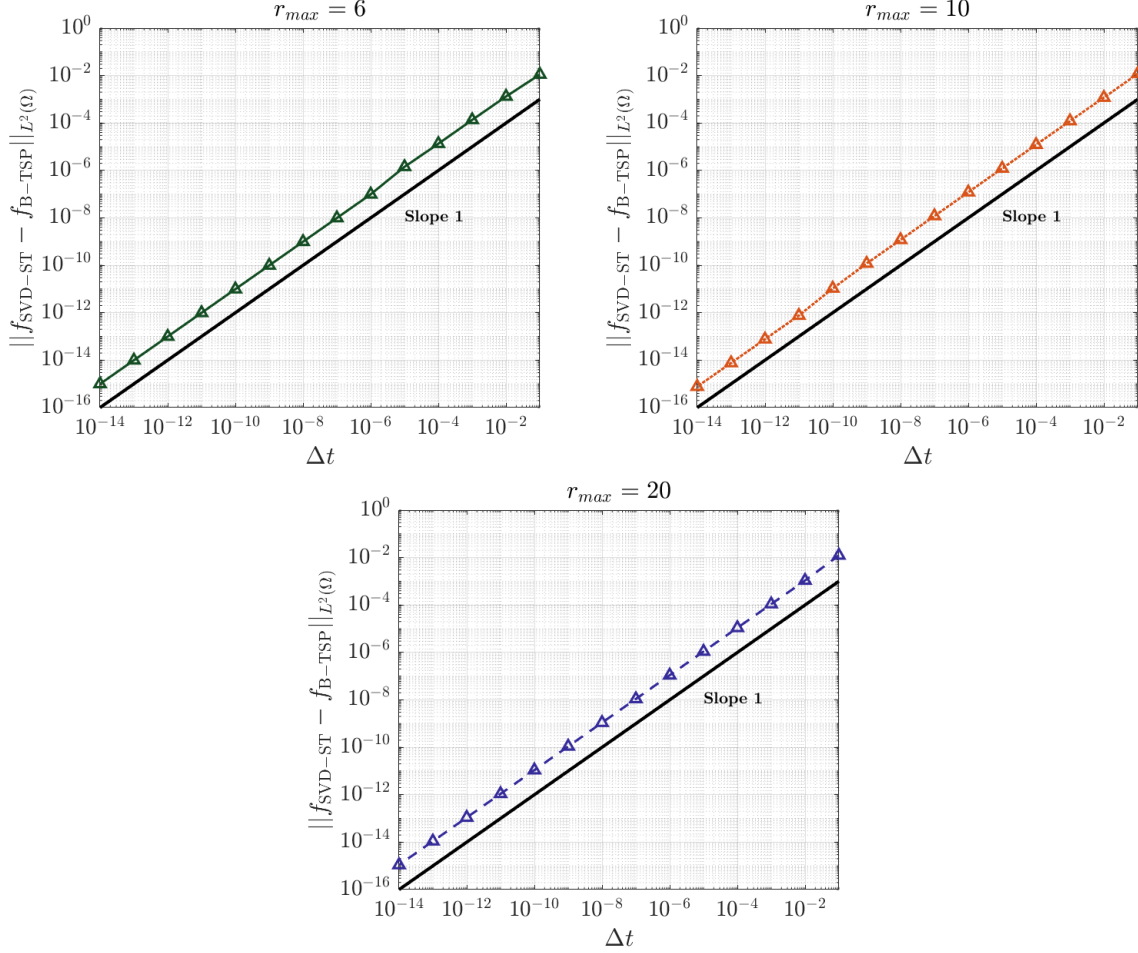


FIG. 8. Numerical demonstration of the sub-optimality of the SVD step-truncation integrator (2.7) applied to the Fokker-Planck equation (6.3) in dimension $d = 4$. Discretization is described in the caption of Figure 7. The integer r_{max} is the maximal rank on a dimension tree after an application of \mathfrak{T}_r^{SVD} to the initial condition u_0 . As shown above, the order is not sufficiently high to indicate that the SVD step-truncation algorithm is consistent with the best step-truncation. For completeness, we have demonstrated this fact for several choices of rank.

for best truncation proven in [14] that the \mathfrak{T}_r^{best} is obtained from truncating the smallest $\min(n_1, n_2) - r$ singular values and singular vectors. For simplicity, we will write down the best truncation scheme for (1.2) using the Euler Forward method. This gives

$$(7.1) \quad \mathbf{f}_{k+1} = \mathfrak{T}_r^{best}(\mathbf{f}_k + \Delta t_k \mathbf{N}(\mathbf{f}_k)).$$

Assuming that we are fixing rank to be the same as the initial condition for all k , we have that $\mathfrak{T}_r^{best}(\mathbf{f}_k) = \mathbf{f}_k$. Now we can apply SVD perturbation theory [26, 41] to express the best truncation operator in terms of a power series expansion in Δt . Representing our decomposition as the a tuple of matrices $(\Sigma_k, \mathbf{Q}_k, \mathbf{V}_k)$, where $\mathbf{f}_k = \mathbf{Q}_k \Sigma_k \mathbf{V}_k^\top$ and $\mathbf{f}_{k+1} = \mathbf{Q}_{k+1} \Sigma_{k+1} \mathbf{V}_{k+1}^\top$ is the reduced singular value decomposition, we have that

$$(7.2) \quad \Sigma_{k+1} = \Sigma_k + \Delta t_k \text{diag}(\mathbf{Q}_k^\top \mathbf{N}(\mathbf{f}_k) \mathbf{V}_k) + O(\Delta t_k^2),$$

$$(7.3) \quad \begin{aligned} \mathbf{Q}_{k+1} &= \mathbf{Q}_k + \Delta t_k \mathbf{Q}_k (\mathbf{H}_k \odot (\mathbf{Q}_k^\top \mathbf{N}(\mathbf{f}_k) \mathbf{V}_k \Sigma_k + \Sigma_k \mathbf{V}_k^\top \mathbf{N}(\mathbf{f}_k)^\top \mathbf{Q}_k)) \\ &\quad + \Delta t_k (\mathbf{I} - \mathbf{Q}_k \mathbf{Q}_k^\top) \mathbf{N}(\mathbf{f}_k) \mathbf{V}_k \Sigma_k^{-1} + O(\Delta t_k^2), \end{aligned}$$

$$(7.4) \quad \begin{aligned} \mathbf{V}_{k+1} &= \mathbf{V}_k + \Delta t_k \mathbf{V}_k (\mathbf{H}_k \odot (\Sigma_k \mathbf{Q}_k^\top \mathbf{N}(\mathbf{f}_k) \mathbf{V}_k + \mathbf{V}_k^\top \mathbf{N}(\mathbf{f}_k)^\top \mathbf{Q}_k \Sigma_k)) \\ &\quad + \Delta t_k (\mathbf{I} - \mathbf{V}_k \mathbf{V}_k^\top) \mathbf{N}(\mathbf{f}_k)^\top \mathbf{Q}_k \Sigma_k^{-1} + O(\Delta t_k^2). \end{aligned}$$

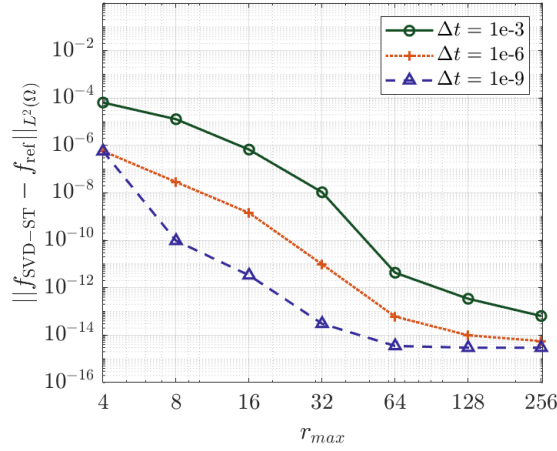


FIG. 9. Numerical demonstration of Corollary 4.2. The numerical grid discretization and described in the caption of Figure 7 and Figure 8. We see that the one step error can be made arbitrarily small, until accuracy of machine arithmetic is reached.

Here, \odot denotes is the element-wise (Hadamard) product of matrices and the matrix

$$(7.5) \quad \begin{cases} \mathbf{H}_k[i, j] = 1/(\Sigma_k[j, j]^2 - \Sigma_k[i, i]^2), & i \neq j \\ \mathbf{H}_k[i, j] = 0 & i = j \end{cases}$$

is skew symmetric and stores information about the differences of the singular values. The $\text{diag}(\cdot)$ operation zeros out all elements of this argument off of the diagonal. The tangent space projection operator is the coefficient of the Δt_k terms. From here, we can see that the evolution equation corresponding to (7.1) is

$$(7.6) \quad \frac{d}{dt} \Sigma = \text{diag}(\mathbf{Q}^\top \mathbf{N}(\mathbf{f}) \mathbf{V}),$$

$$(7.7) \quad \frac{d}{dt} \mathbf{Q} = \mathbf{Q}(\mathbf{H} \odot (\mathbf{Q}^\top \mathbf{N}(\mathbf{f}) \mathbf{V} \Sigma + \Sigma \mathbf{V}^\top \mathbf{N}(\mathbf{f})^\top \mathbf{Q})) + (\mathbf{I} - \mathbf{Q} \mathbf{Q}^\top) \mathbf{N}(\mathbf{f}) \mathbf{V} \Sigma^{-1},$$

$$(7.8) \quad \frac{d}{dt} \mathbf{V} = \mathbf{V}(\mathbf{H} \odot (\Sigma \mathbf{Q}^\top \mathbf{N}(\mathbf{f}) \mathbf{V} + \mathbf{V}^\top \mathbf{N}(\mathbf{f})^\top \mathbf{Q} \Sigma)) + (\mathbf{I} - \mathbf{V} \mathbf{V}^\top) \mathbf{N}(\mathbf{f})^\top \mathbf{Q} \Sigma^{-1}.$$

By setting $\mathbf{U} = \mathbf{Q} \Sigma$ It can be verified that the pair (\mathbf{U}, \mathbf{V}) satisfy the dynamically bi-orthogonal equations of [6]. It should be noted that this is not the only parametrization of the fixed rank solution $\mathbf{f} = \mathbf{Q} \Sigma \mathbf{V}^\top$. Of particular interest is the closely related projection method given by the DDO approximation (equivalent to HT tangential dynamics in 2D)

$$(7.9) \quad \frac{d}{dt} \mathbf{A} = \mathbf{W}^\top \mathbf{N}(\mathbf{f}) \mathbf{B},$$

$$(7.10) \quad \frac{d}{dt} \mathbf{W} = (\mathbf{I} - \mathbf{W} \mathbf{W}^\top) \mathbf{N}(\mathbf{f}) \mathbf{B} \mathbf{A}^{-1},$$

$$(7.11) \quad \frac{d}{dt} \mathbf{B} = (\mathbf{I} - \mathbf{B} \mathbf{B}^\top) \mathbf{N}(\mathbf{f})^\top \mathbf{W} \mathbf{A}^{-\top}.$$

Which is equivalent to the SVD equations above in the sense that

$$(7.12) \quad \mathbf{W}(t) \mathbf{A}(t) \mathbf{B}^\top(t) = \mathbf{f}(t) = \mathbf{Q}(t) \Sigma(t) \mathbf{V}^\top(t)$$

as long as the singular values are distinct and the equation holds at $t = 0$. A comparison of methods for fixed rank initial value problems is given in [31].

Appendix B: Hierarchical Tucker tensor format and its parallel implementation. For the purposes of introducing a general software for computing on Hierarchical Tucker and related rank-restricted spaces of tensors, we have developed a parallel implementation of some basic functions of the Hierarchical Tucker format. Our implementation takes partial inspiration from [15], in that it assigns each node on a dimension tree to an OpenMPI rank. The implementation we have developed shares a considerable amount of its design with our previous software package [35]. However our new software is written entirely in C with an alternative memory management model and struct implementations. This allowed for incorporating the geometric structure of the rank constrained manifolds into the software design, rather than trying to build around our previous design choices.

We will give a brief overview of the software implementation for the Tangent Projector function, as this is the core feature which allows us to treat the Hierarchical Tensors of fixed rank as points on a manifold. We assume that the tensor we wish to project onto the tangent space has is in the HTucker format with the same tree structure as our manifold, but with possibly different ranks. Our implementation follows the outline given by [28] in Section 7.2. Rather than recount their algorithm verbatim, as this is the fundamental result of their paper, we will discuss parallel implementation specifics. We first ensure that all the basis matrices for the tree are orthogonal, so as to guarantee the tangent space parametrization of [8] and [43] is used. Afterward, we compute the gram matrices \mathbf{G}_t of [14]. (For orthogonalized HT tensors, the gram matrices are equivalent to equations (3.11) and (3.12) of [28]. See Algorithm 3 of [25] for numerical detail.) Next, a sequence of HT format inner product intermediate matrices are computed, identically to Algorithm 2 of [25]. Each of these are computed using OpenMP message passes in parallel. The most numerically sensitive part of the projection is the inversion of the gram matrices. Assuming that each \mathbf{G}_t is well conditioned, there is no issue. However if this is not the case, this geometrically indicates that our current point on the manifold is numerically close to the boundary, which is a union of the cases of all such lower rank \mathbf{G}_t . Thus, we must either truncate the current point or solve the matrix inverse problem taking this poor conditioning into account. First, consider the case where we choose to truncate to the boundary. To do so, we look at the spectrum of the self-adjoint matrix \mathbf{G}_t . We drop every eigenpair with $\lambda < \varepsilon_{tolerance}$. One slightly more efficient approach would incorporate this eigenvalue dropping directly into the matrix inversion problem. Fortunately, LAPACK [1] has a routine specifically for this purpose. The routine DGELSS solves a rank-deficient least squares problem by dropping the poorly conditioned singular values of the input matrix to be inverted. Using this routine, we have automatic detection of poor rank conditioning so that a numerically stable solution is chosen. Moreover, the solution computed by the least squares problem can be immediately used for cases where we have no issues on rank conditioning. Once all inverses are computed, the final projection steps shown in (3.15), (3.16), (3.17) of [28]. The array of matrices representing the an HTucker tangent vector are stored in distributed memory convention using MPI, just as the points on the manifold are stored. From here, a tangent is immediately ready for computation in a rank constrained temporal integrator.

REFERENCES

- [1] E. ANDERSON, Z. BAI, C. BISCHOF, S. BLACKFORD, J. DEMMEL, J. DONGARRA, J. DU CROZ, A. GREENBAUM, S. HAMMARLING, A. MCKENNEY, AND D. SORENSEN, *LAPACK Users' Guide*, Society for Industrial and Applied Mathematics, Philadelphia, PA, third ed., 1999.
- [2] M. BACHMAYR, R. SCHNEIDER, AND A. USCHMAJEV, *Tensor networks and hierarchical tensors for the solution of high-dimensional partial differential equations*, Foundations of Computational Mathematics, 16 (2016).
- [3] V. BARTHELMANN, E. NOVAK, AND K. RITTER, *High dimensional polynomial interpolation on sparse grids*, Advances in Computational Mechanics, 12 (2000), pp. 273–288.
- [4] A. M. P. BOELENS, D. VENTURI, AND D. M. TARTAKOVSKY, *Parallel tensor methods for high-dimensional linear PDEs*, J. Comput. Phys., 375 (2018), pp. 519–539.
- [5] H. J. BUNGARTZ AND M. GRIEBEL, *Sparse grids*, Acta Numerica, 13 (2004), pp. 147–269.
- [6] M. CHENG, T. Y. HOU, AND Z. ZHANG, *A dynamically bi-orthogonal method for time-dependent stochastic partial differential equations i: Derivation and algorithms*, Journal of Computational Physics, 242 (2013), pp. 843–868.
- [7] A. CHKIFA, A. COHEN, AND C. SCHWAB, *High-dimensional adaptive sparse polynomial interpolation and applications to parametric PDEs*, Found. Comput. Math., 14 (2014), pp. 601–633.
- [8] C. DA SILVA AND F. J. HERRMANN, *Optimization on the hierarchical tucker manifold—applications to tensor completion*, Linear Algebra and its Applications, 481 (2015), pp. 131–173.
- [9] A. DEKTOR AND D. VENTURI, *Dynamical tensor approximation of high-dimensional nonlinear pdes*, ArXiv, 2007.09538 (2020), pp. 1–23.
- [10] A. DEKTOR AND D. VENTURI, *Dynamically orthogonal tensor methods for high-dimensional nonlinear pdes*, Journal of

- Computational Physics, 404 (2020), p. 109125.
- [11] W. E, J. HAN, AND Q. LI, *A mean-field optimal control formulation of deep learning*, Res. Math. Sci., 6 (2019), pp. 1–41.
 - [12] J. FOO AND G. E. KARNIADAKIS, *Multi-element probabilistic collocation method in high dimensions*, J. Comput. Phys., 229 (2010), pp. 1536–1557.
 - [13] W. GANGBO, W. LI, S. OSHER, AND M. PUTHAWALA, *Unnormalized optimal transport*, J. Comput. Phys., 399 (2019), p. 108940.
 - [14] L. GRASEDYCK, *Hierarchical singular value decomposition of tensors*, SIAM Journal on Matrix Analysis and Applications, 31 (2010), pp. 2029–2054.
 - [15] L. GRASEDYCK AND C. LÖBBERT, *Distributed hierarchical SVD in the hierarchical Tucker format*, Numer. Linear Algebra Appl., 25 (2018), p. e2174.
 - [16] W. HACKBUSCH, *Tensor spaces and numerical tensor calculus*, Springer, 2012.
 - [17] J. S. HESTHAVEN, S. GOTTLIEB, AND D. GOTTLIEB, *Spectral methods for time-dependent problems*, Cambridge University Press, 2007.
 - [18] S. HOLTZ, T. ROHWEDDER, AND R. SCHNEIDER, *On manifolds of tensors of fixed TT-rank*, Numer. Math., 120 (2012), pp. 701–731.
 - [19] L. KARLSSON, D. KRESSNER, AND A. USCHMAJEV, *Parallel algorithms for tensor completion in the CP format*, Parallel computing, 57 (2016), pp. 222–234.
 - [20] B. N. KHOROMSKIJ, *Tensor numerical methods for multidimensional PDEs: theoretical analysis and initial applications*, in CEMRACS 2013—modelling and simulation of complex systems: stochastic and deterministic approaches, vol. 48 of ESAIM Proc. Surveys, EDP Sci., Les Ulis, 2015, pp. 1–28.
 - [21] V. I. KLYATSKIN, *Dynamics of stochastic systems*, Elsevier Publishing Company, 2005.
 - [22] O. KOCH AND C. LUBICH, *Dynamical low-rank approximation*, SIAM Journal on Matrix Analysis and Applications, 29 (2007), pp. 434–454.
 - [23] O. KOCH AND C. LUBICH, *Dynamical tensor approximation*, SIAM J. Matrix Anal. Appl., 31 (2010), pp. 2360–2375.
 - [24] T. KOLDA AND B. W. BADER, *Tensor decompositions and applications*, SIREV, 51 (2009), pp. 455–500.
 - [25] D. KRESSNER AND C. TOBLER, *Algorithm 941: htucker – a Matlab toolbox for tensors in hierarchical Tucker format*, ACM Transactions on Mathematical Software, 40 (2014), pp. 1–22.
 - [26] J. LIU, X. LIU, AND X. MA, *First-order perturbation analysis of singular vectors in singular value decomposition*, IEEE Transactions on Signal Processing, 56 (2008), pp. 3044–3049.
 - [27] C. LUBICH AND I. V. OSELEDETS, *A projector-splitting integrator for dynamical low-rank approximation*, BIT Numerical Mathematics, 54 (2014), pp. 171–188.
 - [28] C. LUBICH, T. ROHWEDDER, R. SCHNEIDER, AND B. VANDEREYCKEN, *Dynamical approximation by hierarchical tucker and tensor-train tensors*, SIAM Journal on Matrix Analysis and Applications, 34 (2013), pp. 470–494.
 - [29] T. MARZ AND C. B. MACDONALD, *Calculus on surfaces with general closest point functions*, SIAM Journal on Numerical Analysis, 50 (2012), pp. 3303–3328.
 - [30] X. MENG, Z. LI, D. ZHANG, AND G. KARNIADAKIS, *Ppinn: Parareal physics-informed neural network for time-dependent pdes*, Computer Methods in Applied Mechanics and Engineering, 370 (2020), p. 113250, <https://doi.org/10.1016/j.cma.2020.113250>.
 - [31] E. MUSHARBASH, F. NOBILE, AND T. ZHOU, *Error analysis of the dynamically orthogonal approximation of time dependent random pdes*, SIAM Journal on Scientific Computing, 37 (2015), pp. A776–A810.
 - [32] A. NARAYAN AND J. JAKEMAN, *Adaptive Leja sparse grid constructions for stochastic collocation and high-dimensional approximation*, SIAM J. Sci. Comput., 36 (2014), pp. A2952–A2983.
 - [33] M. RAISSI AND G. E. KARNIADAKIS, *Hidden physics models: Machine learning of nonlinear partial differential equations*, J. Comput. Phys., 357 (2018), pp. 125–141.
 - [34] M. RAISSI, P. PERDIKARIS, AND G. E. KARNIADAKIS, *Physics-informed neural networks: A deep learning framework for solving forward and inverse problems involving nonlinear partial differential equations*, J. Comput. Phys., 378 (2019), pp. 606–707.
 - [35] A. RODGERS, *htucker-mpi*. <https://github.com/akrodger/htucker-mpi>, 2019.
 - [36] A. RODGERS AND D. VENTURI, *Stability analysis of hierarchical tensor methods for time-dependent pdes*, Journal of Computational Physics, 409 (2020), p. 109341.
 - [37] T. ROHWEDDER AND A. USCHMAJEV, *On local convergence of alternating schemes for optimization of convex problems in the tensor train format*, SIAM J. Numer. Anal., 51 (2013), pp. 1134–1162.
 - [38] L. RUTHOTTO, S. OSHER, W. LI, L. NURBEKYAN, AND S. W. FUNG, *A machine learning framework for solving high-dimensional mean field game and mean field control problems*, PNAS, 117 (2020), pp. 9183–9193.
 - [39] T. P. SAPSIS AND P. F. LERMUSIAUX, *Dynamically orthogonal field equations for continuous stochastic dynamical systems*, Physica D: Nonlinear Phenomena, 238 (2009), pp. 2347–2360.
 - [40] R. SCHNEIDER AND A. USCHMAJEV, *Approximation rates for the hierarchical tensor format in periodic sobolev spaces*, Journal of complexity, 30 (2014), pp. 56–71, <https://doi.org/10.1016/j.jco.2013.10.001>.
 - [41] G. W. STEWART, *Perturbation theory for the singular value decomposition*, tech. report, 1998.
 - [42] J. C. STRIKWERDA, *Finite difference schemes and partial differential equations*, SIAM, second ed., 2004.
 - [43] A. USCHMAJEV AND B. VANDEREYCKEN, *The geometry of algorithms using hierarchical tensors*, Linear Algebra and its Applications, 439 (2013), pp. 133–166.
 - [44] D. VENTURI, *The numerical approximation of nonlinear functionals and functional differential equations*, Physics Reports, 732 (2018), pp. 1–102.
 - [45] D. VENTURI AND A. DEKTOR, *Spectral methods for nonlinear functionals and functional differential equations*, ArXiv, 1909.07960 (2020), pp. 1–34.
 - [46] D. VENTURI AND G. E. KARNIADAKIS, *Convolutionless Nakajima-Zwanzig equations for stochastic analysis in nonlinear dynamical systems*, Proc. R. Soc. A, 470 (2014), pp. 1–20.

- [47] D. VENTURI, T. P. SAPSIS, H. CHO, AND G. E. KARNIADAKIS, *A computable evolution equation for the joint response-excitation probability density function of stochastic dynamical systems*, Proc. R. Soc. A, 468 (2012), pp. 759–783.
- [48] C. VILLANI, *Optimal transport: old and new*, Springer, 2009.
- [49] Y. ZHU, N. ZABARAS, P.-S. KOUTSOURELAKIS, AND P. PERDIKARIS, *Physics-constrained deep learning for high-dimensional surrogate modeling and uncertainty quantification without labeled data*, J. Comput. Phys., 394 (2019), pp. 56–81.